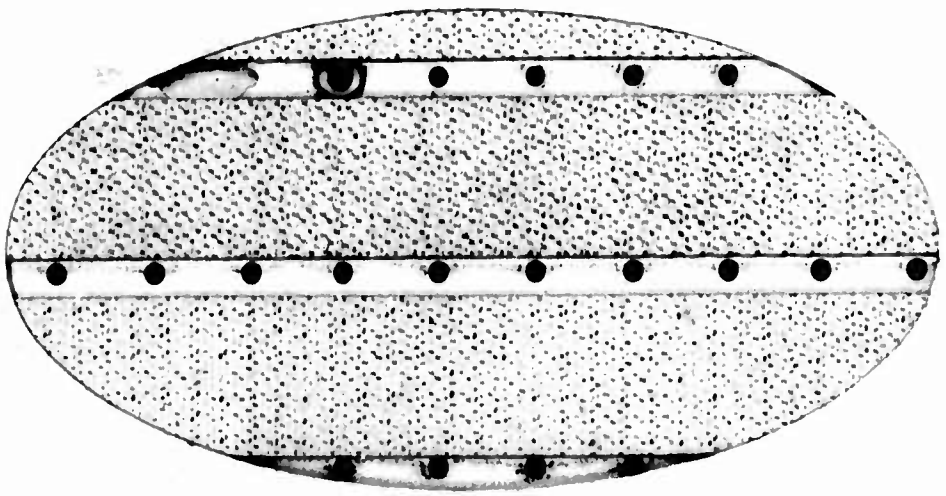

EPCO ENGINEERING-PHYSICS COMPANY
5618 RANDOLPH ROAD / ROCKVILLE, MARYLAND

ENGINEERING-PHYSICS COMPANY
5515 Randolph Road
Rockville, Maryland

THREE-DIMENSIONAL ANALYSIS OF BULK CAVITATION -- INTERIM REPORT

by Vincent Cushing, George Bowden, and Dean Reily

For

OFFICE OF NAVAL RESEARCH

Washington, D. C.

Contract NONR-3709(00)
EPCO Project No. 106

September 24, 1962

TABLE OF CONTENTS

FOREWORD

This is an interim report on the three-dimensional analysis of bulk cavitation and secondary water hammer which is being conducted for the Office of Naval Research under contract NONR-3709(00).

In work already carried out by one of the authors for the Office of Naval Research, there has been conducted and reported a study of the mechanics or physics of bulk cavitation for the one-dimensional case; the work now reported is the three-dimensional embellishment.

We find that, for practicable ranges of yield and depth of burst, the size, location, and shape of the cavitated region appears to be quite different from that which has been traditionally accepted.

The portion of the analysis bearing on closure and secondary waves is still in process, and so is not reported herein; however, as a preliminary, we do report on the rudimentary analysis of the trajectory of the water hammer. We also make a general discussion of the secondary wave configurations which one might expect to be associated with such a traveling hammer.

We are particularly appreciative of the assistance to our theoretical effort which has been provided by Dr. Heinrich Schauer and his associates at the Underwater Explosives Research Division--especially the help provided by a preliminary analysis of their very recent bulk cavitation experiments. Past widespread observations of bulk cavitation phenomena have been most helpful throughout this investigation, and we are most grateful for the assistance in

this regard which has continually been provided by Dr. William Murray of the David Taylor Model Basin and Dr. E. H. Swift, Jr., of the Naval Ordnance Laboratory. We are also grateful for the support and continual assistance provided by the project scientific officer, Mr. James Winchester of the Office of Naval Research.

Respectfully submitted,

ENGINEERING-PHYSICS COMPANY

Vincent J. Cushing

George E. Bowden

Dean M. Reily

THREE-DIMENSIONAL ANALYSIS OF BULK CAVITATION -- INTERIM REPORT

I. INTRODUCTION

This is an interim technical report of work conducted under Contract NONR-3709(00). The work now being conducted is a three-dimensional embellishment of previous work conducted, the final report of which has already been submitted.[1] The overall subject matter has consisted of an investigation of the underlying theory as well as some of the practicable aspects associated with bulk cavitation and subsequent secondary pressure waves which have been observed in connection with underwater detonations of conventional high explosives as well as nuclear explosives.

To date in the three-dimensional effort we have completed, and report herein, the detailed analysis--together with machine computational results--bearing on the extent of the cavitated region as a function of depth of burst and yield. The rigorous or detailed analysis bearing on closure and secondary waves is still in process, and so is not discussed in this report; however, as a preliminary to the detailed closure analysis, we have carried out and report herein a rudimentary analysis of the expected water hammer and its associated secondary wave configuration.

In particular in the work completed so far we have found that the extent of the cavitated region is quite different in size, location, and shape from that which had been traditionally accepted. There has never been an explicit

---

[1] Vincent Cushing, "Study of Bulk Cavitation and Consequent Water Hammer," Final Report to Contract NONR-3389(00) for Office of Naval Research, October 31, 1961.

bulk cavitation experimental investigation,* and so it is not surprising that the rather casual indirect observations of bulk cavitation have not portrayed either the extent or variety of cavitation which has been found in our models.

Bulk cavitation is a phenomenon similar to that of spallation; it occurs whenever a strong compression wave reflects from a free surface. The reflected wave, a rarefaction wave, can give rise to large net tensions throughout a large region of the water; since seawater cannot withstand such large tensions the water parts or ruptures, spalling layers of water upward. Later, under the influence of gravitational and other forces, this spalled water again falls back and impacts with the underlying unruptured water. This impact or reloading is tantamount to a large water hammer, which sets up strong secondary waves. Indirect observation, in connection with past underwater explosion tests, have indicated that these secondary waves probably play a large role in the airblast associated with such explosions, and also play a large role in the damage sustained by an underwater or surface vessel.

Our analysis, substantiated by reassessment of past field test results, indicates that a very large fraction (as high as 70-90 per cent) of the total hydrodynamic yield of an underwater explosion is (at least momentarily) absorbed in the cavitation process--and this absorbed energy is later re-emitted in the water hammer at the time of reloading. This absorption and re-emission process transforms completely the character (including wave shape and wave patterns) of

---

*With the exception of a test conducted in June, 1962 by the Underwater Explosives Research Division of the David Taylor Model Basin. At the time of writing, data reduction and analysis on this test data is just commencing, and so no results or conclusions are available now.

the compression or shock wave originating from an underwater explosion.

The overall cavitated region does not close everywhere simultaneously. Actually, closure and water hammer first occur (under most conditions) along the circumference of a circle, the (horizontal) radius of which is a function of yield and depth of burst; thereafter the impact point or water hammer spreads horizontally outward and horizontally inward from this so-called ring of first impact. In effect, then, we have a traveling water hammer configuration, and this traveling water hammer gives rise to secondary wave patterns. The net effect of this traveling water hammer is that the generated secondary wave is generally focused toward two points lying on the vertical axis passing through the explosion: one focal point appears to lie well beneath the burst point, whereas the second focal point lies above the water surface, and thus the reloading secondary wave pattern can give rise to large air pressures in the region generally above surface zero.

In this report we indicate the machine computational results based on a rigorous analysis, which describes the overall extent of cavitation as a function of depth of burst and yield. In the continuing work, we have set up the analysis and are carrying out computations to describe the motion of the cavity boundaries during the closure process; and ultimately describe the water hammer and secondary wave pattern set up at the time of final closure.

II. ANALYTICAL MODEL

For this study, it is assumed that an explosion takes place underwater and that the initial disturbance is a function of radial distance from the source (and not a function of angular position). For a small disturbance and an adiabatic expansion, the equation of motion is

$$\frac{\partial \bar{v}}{\partial t} = -\frac{1}{\rho_o} \text{grad } P \quad , \qquad (1)$$

and the equation of continuity is

$$\frac{1}{c_o^2} \frac{\partial P}{\partial t} = -\rho_o \text{ div } \bar{v} \quad , \qquad (2)$$

where $\bar{v}$ = velocity of the fluid at any point;

ρ_o = density of the fluid;

c_o = speed of sound in the fluid;

P = pressure in the fluid at any point.

For the case to be considered, it is convenient to use spherical coordinates with origin at the source, and the assumptions expressed mathematically become

$$\bar{v} = u_r \frac{\bar{r}}{r}; \quad \frac{\partial P}{\partial \theta} = \frac{\partial P}{\partial \varphi} = 0 \quad . \qquad (3,4)$$

Under these conditions, the equations of motion and continuity become

$$\frac{\partial u_r}{\partial t} = -\frac{1}{\rho_o} \frac{\partial P}{\partial r} \quad ; \qquad (5)$$

$$\frac{1}{c_o^2} \frac{\partial P}{\partial t} = -\rho_o \frac{1}{r^2} \frac{\partial}{\partial r} (r^2 u_r) \quad . \qquad (6)$$

If u_r, the particle velocity, is eliminated, then

$$\frac{1}{r^2}\frac{\partial}{\partial r}\left(r^2\frac{\partial P}{\partial r}\right) = \frac{1}{c_o^2}\frac{\partial^2 P}{\partial t^2} \quad . \tag{7}$$

Any function of the form,

$$P(r,t) - P_o = \frac{1}{r} f\,(t - r/c_o) \quad , \tag{8}$$

is a solution of this equation.

If this result is substituted into the equation of motion, then

$$u_r(t) - u_r(t_o) = \frac{P - P_o}{\rho_o c_o} + \frac{1}{\rho_o r}\int_{t_o}^{t} [P(r,t') - P_o]dt' \quad . \tag{9}$$

At this point, it can be observed that, although the form of the spherical wave does not change as it spreads out, its amplitude decreases due to the factor $\frac{1}{r}$. Also, the particle velocity does not become zero when the pressure returns to the equilibrium value, but will continue to have a positive value due to the integral term. The development so far has directly followed that of Cole.[2]

Now, if the wave is assumed to be a shock front with exponential decay,

$$f(t - r/c_o) = \begin{cases} A\, e^{-b(t - r/c_o)} & ;\ t - r/c_o \geq 0 \\ 0 & ;\ t - r/c_o < 0 \end{cases} \quad , \tag{10}$$

---

[2] Robert H. Cole, Underwater Explosions, Princeton Univ. Press, Princeton, N. J., 1948.

and
$$P(r,t) - P_o = \begin{cases} \frac{A}{r} e^{-b(t - r/c_o)} & ; \; t - r/c_o \geq 0 \\ 0 & ; \; t - r/c_o < 0 \end{cases} . \qquad (11)$$

If $t = t_o$ is assumed to be a time before the explosion, then $u_r(t_o) = 0$ and

$$u_r(t) = \begin{cases} \frac{A}{r\rho_o c_o} e^{-b(t - r/c_o)} + \frac{A}{\rho_o r^2 b} [1 - e^{-b(t - r/c_o)}] & ; \; t - r/c_o \geq 0 \\ 0 & ; \; t - r/c_o < 0 \end{cases} \qquad (12)$$

It can be seen that b corresponds to $\frac{1}{\tau}$ and $\frac{b}{c_o}$ corresponds to $\frac{1}{\lambda}$ as used in the one-dimensional analysis already reported.[3] Furthermore, $P(r,t) - P_o$ corresponds to P_1 in the earlier report, or, in other words, P_1 represented the increase in pressure above equilibrium. Now, if the depth of the explosion is d, then $A = P_s d$, then where P_s is the maximum increase of pressure above equilibrium at the point on the surface directly above the explosion. If these substitutions are made, the above equations become

$$P_1 = \begin{cases} \frac{P_s d}{r} e^{-(t/\tau - r/\lambda)} & ; \quad t/\tau - r/\lambda \geq 0 \\ 0 & ; \quad t/\tau - r/\lambda < 0 \end{cases} , \qquad (13)$$

$$u_r = \begin{cases} \frac{P_s d}{r\rho_o c_o} e^{-(t/\tau - r/\lambda)} + \frac{P_s d\tau}{\rho_o r^2} [1 - e^{-(t/\tau - r/\lambda)}] & ; t/\tau - r/\lambda \geq 0 \\ 0 & ; t/\tau - r/\lambda < 0 \end{cases} . \qquad (14)$$

---

[3] Vincent Cushing, loc. cit.

Now, as in the previous work, let $T = t/\tau$, $R = r/\lambda$ and $P = P/\rho_o c_o$ and, in addition, let $d/\lambda = D$, then

$$P_1 = \begin{cases} \frac{P_s D}{R} e^{-(T - R)} & T - R \geq 0 \\ 0 & T - R < 0 \end{cases} , \quad (15)$$

$$u_r = \begin{cases} \frac{P_s D}{R} e^{-(T - R)} + \frac{P_s D}{R^2} \left[1 - e^{-(T - R)}\right] & T - R \geq 0 \\ 0 & T - R < 0 \end{cases} . \quad (16)$$

One essential difference between the three-dimensional case and the one-dimensional case must be noted, T is equal to zero at the time at which the shock front would have left the source had it traveled at sonic velocity throughout its path in this case, whereas, in the one-dimensional case T was equal to zero at the time at which the front reached the surface.

When the disturbance reaches the free surface, it is reflected back as a rarefaction. However, in the three-dimensional case, the front does not approach the surface normally in general. The reflection is, therefore, not, in general, along the same path as the initial wave, but along a line forming an angle of the same magnitude with the normal to the surface as the impinging disturbance but with opposite sign. The reflection thus follows the familiar Snell's Law of Reflection. If the surface is assumed to be a horizontal straight line, the reflected wave can be thought of as emanating from a point on the same vertical line as the original source at a distance, D, above the

surface, the so-called "mirror image" of the source. If R_1 is distance from the imaginary or virtual source and a the angle between a given ray and the vertical, then P_2, the pressure or tension (since it is a negative pressure) in the reflected wave, is given by

$$P_2 = \begin{cases} -\frac{P_s D}{R_1} e^{-(T - R_1)} & T - R_1 \geq 0, \text{ and } R_1 \cos a \geq D \\ 0 & \text{otherwise} \end{cases} \quad . \quad (17)$$

The geometry of this situation is sketched in Fig. 1.

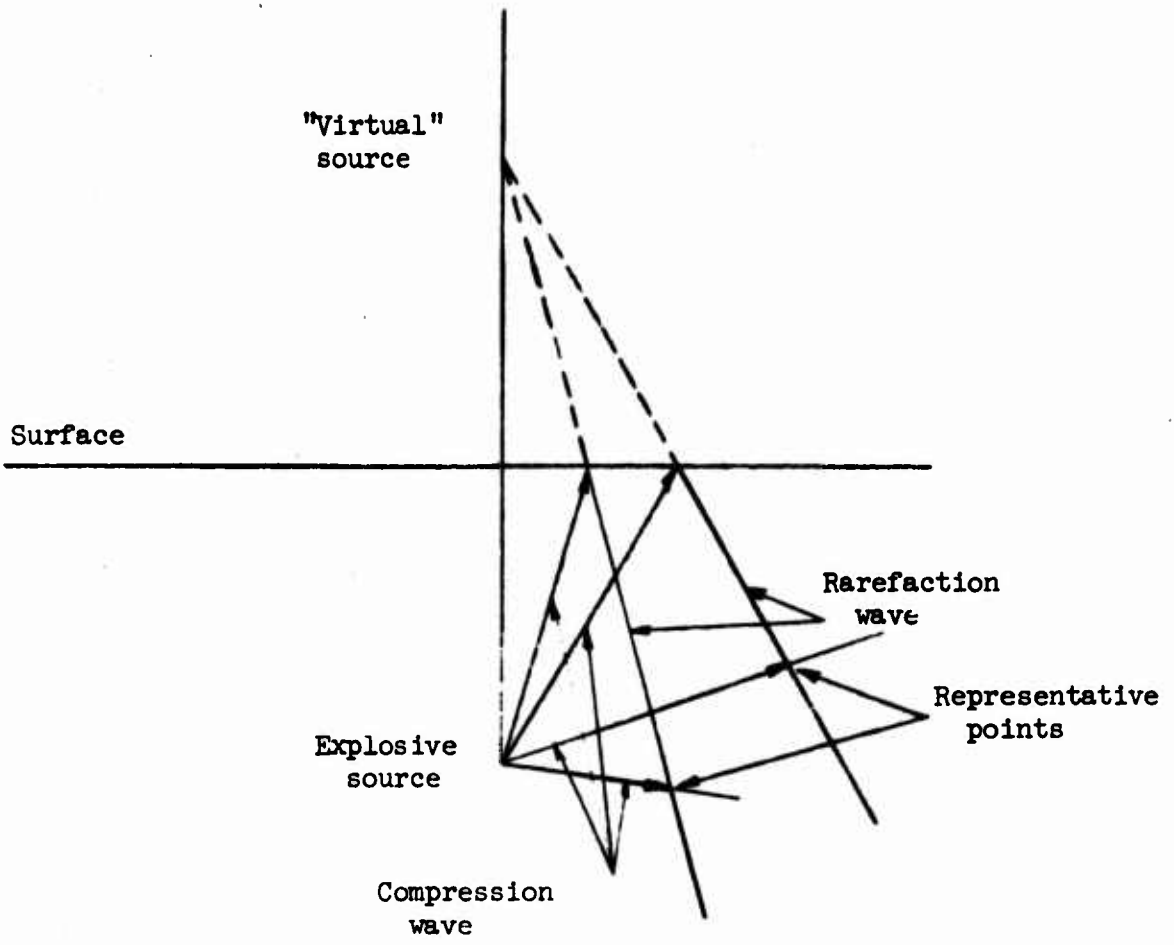

Fig. 1--Sketch of underwater explosion illustrating force field.

III. PRESSURE FIELD WITHOUT CAVITATION

Based on the model developed in Section II above, the total pressure at any point within the fluid can be determined as the algebraic sum of

1. the compression wave emanating from the source of the explosion;
2. the rarefaction wave caused by the reflection of this pressure wave at the surface of the fluid;
3. hydrostatic pressure;
4. atmospheric pressure.

If a coordinate system is set up in the fluid such that the z coordinate is measured downward from the surface and the h coordinate is measured horizontally from the point of the explosion (since it is assumed that the explosion is spherically symmetric, there is no need to have but a single horizontal coordinate as the pressure field will be cylindrically symmetric around the vertical line through the explosion), the total pressure at any point (z,h) at any time, t, is given by

$$P_t(z,h,t) = \begin{cases} gz + P_a & ; \quad t < r/c_o \\ \dfrac{P_s d}{r} e^{-(t - r/c_o)/\tau} + gz + P_a & ; \quad r_o/c_o \le t < r_1/c_o \\ P_s d\left[\dfrac{e^{-(t - r/c_o)/\tau}}{r} - \dfrac{e^{-(t - r_1/c_o)/\tau}}{r_1}\right] + gz + P_a & ; \quad t \ge r_1/c_o \end{cases} \qquad (18)$$

where $r^2 = (d - z)^2 + h^2$;

$r_1^2 = (d + z)^2 + h^2$;

t_a is the atmospheric pressure;

g is the weight per unit volume of the fluid; and

P_s, d, and c_o are as defined in the previous section.

The total pressure may be expressed in a dimensionless form and it is in this form that the calculations completed so far have been made. To obtain the dimensionless form, each pressure is divided by P_s, each length is divided by $\tau\, c_o$ and the time is divided by τ. Equation (1) then becomes

$$P_t(z,h,t) = \begin{cases} Gz + P_a & ; \quad t < r \\ \frac{d}{r}\, e^{-(t - r)} + Gz + P_a & ; \quad r \leq t < r_1 \\ d\left[\frac{e^{-(t - r)}}{r} - \frac{e^{-(t - r_1)}}{r_1}\right] + Gz + P_a & ; \quad t \geq r_1 \end{cases} , \tag{19}$$

where each of the quantities is now dimensionless. The only tricky constant is the G which is equal to the g times $\tau\, c_o$ divided by P_s.

Since this study is concerned primarily with cavitation and since it is known that the presence of cavitation is caused by a negative pressure or tension, the time of particular interest at any point is that time at which the rarefaction wave is at its maximum; since the wave being considered has a shock front and exponential tailoff, this is the time at which the rarefaction front has just reached the point being considered. This time, of course, in the dimensionless presentation of the equation is the time at which t equals r_1. The pressure at this time at any point (z,h) is given by

$$P_t(z,t) = d\left[\frac{e^{-(r_1 - r)}}{r} - \frac{1}{r_1}\right] + Gz + P_a \quad , \tag{20}$$

where all the quantities are in dimensionless form.

Equation (20), then, expresses a function which must be studied to determine the presence of cavitation although it must be noted that the function itself is derived on the tacit assumption that cavitation does not exist. Cavitation will begin when P_t becomes negative and equal to a negative pressure P_b, the breaking or rupture pressure. However, it must be remembered that the rarefaction wave travels along a ray emanating from a "virtual" source above the water. Therefore we wish to study this function as it varies with r_1 or along a given ray from the virtual source.

Representative curves showing the variation of P_t with r_1 are shown in Figs. 2, 3, and 4. It can be seen in Fig. 3 that, if the ray being studied passes sufficiently near the actual source of the explosion, P_t is positive at the surface, becomes negative, reaching a minimum, and rises to a large positive value at or near the explosion, then decreases perhaps becoming negative again reaching a minimum and then rising as r_1 increases until eventually the hydrostatic pressure becomes the dominant term. On the other hand if a ray further removed from the explosion is followed, the value of P_t is still slightly positive at the surface then becomes negative reaching a minimum, and then begins to rise becoming positive and approaching the hydrostatic pressure as r_1 increases. It is perhaps obvious that if a ray so far removed that no effects of the explosion could be discernible were followed then P_t would begin at its surface value and just increase due to hydrostatic pressure.

In order to determine horizontal extent for the cavitated region the expression P_t was expanded in power series assuming that h was much greater than d and z and the point at which the derivative of P_t with respect to r_1

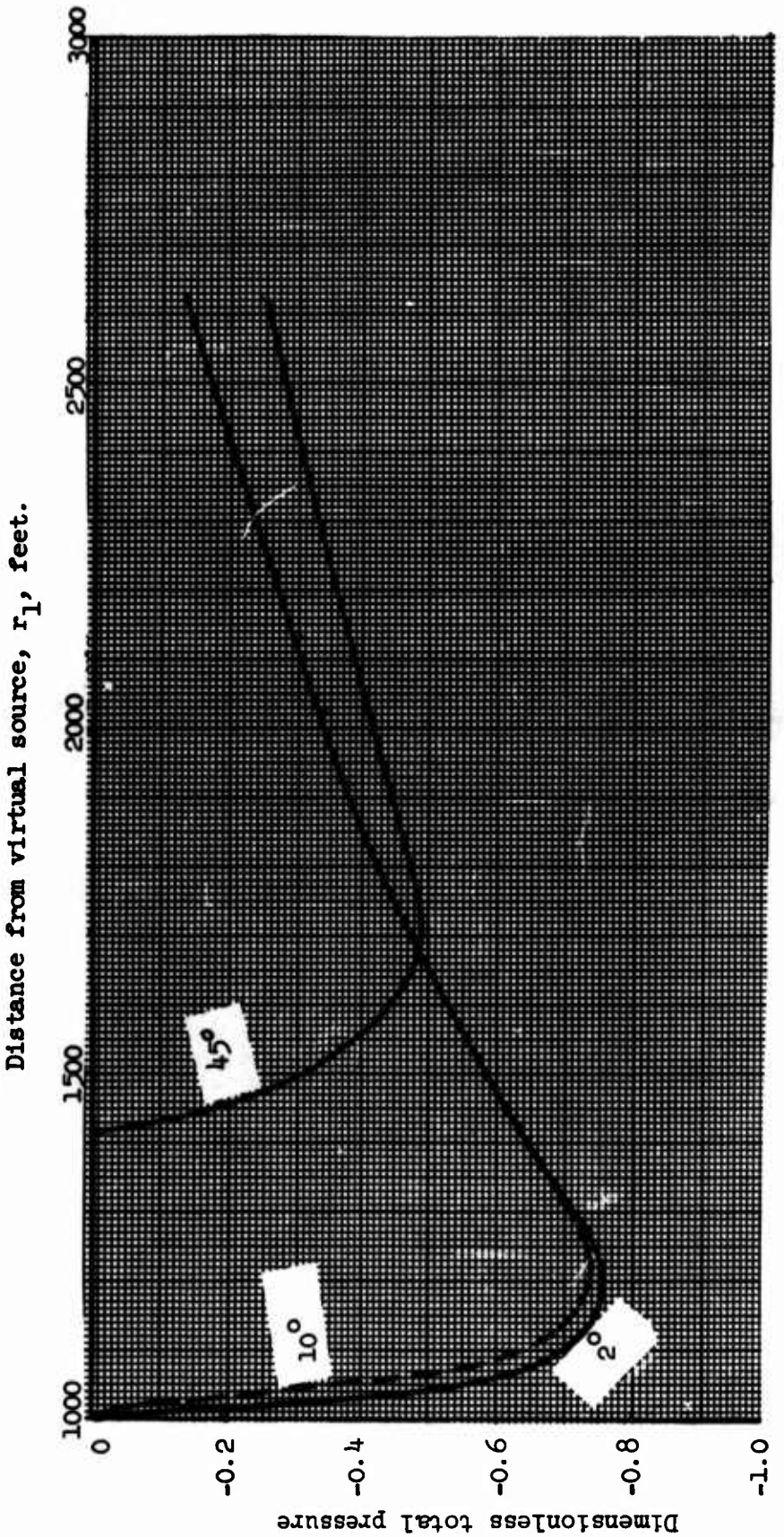

Fig. 2--Dimensionless total pressure as a function of distance from "virtual" source at time of maximum tension for angles of 2°, 10°, and 45° from the vertical. Burst depth = 1000 ft, yield = 10 KT.

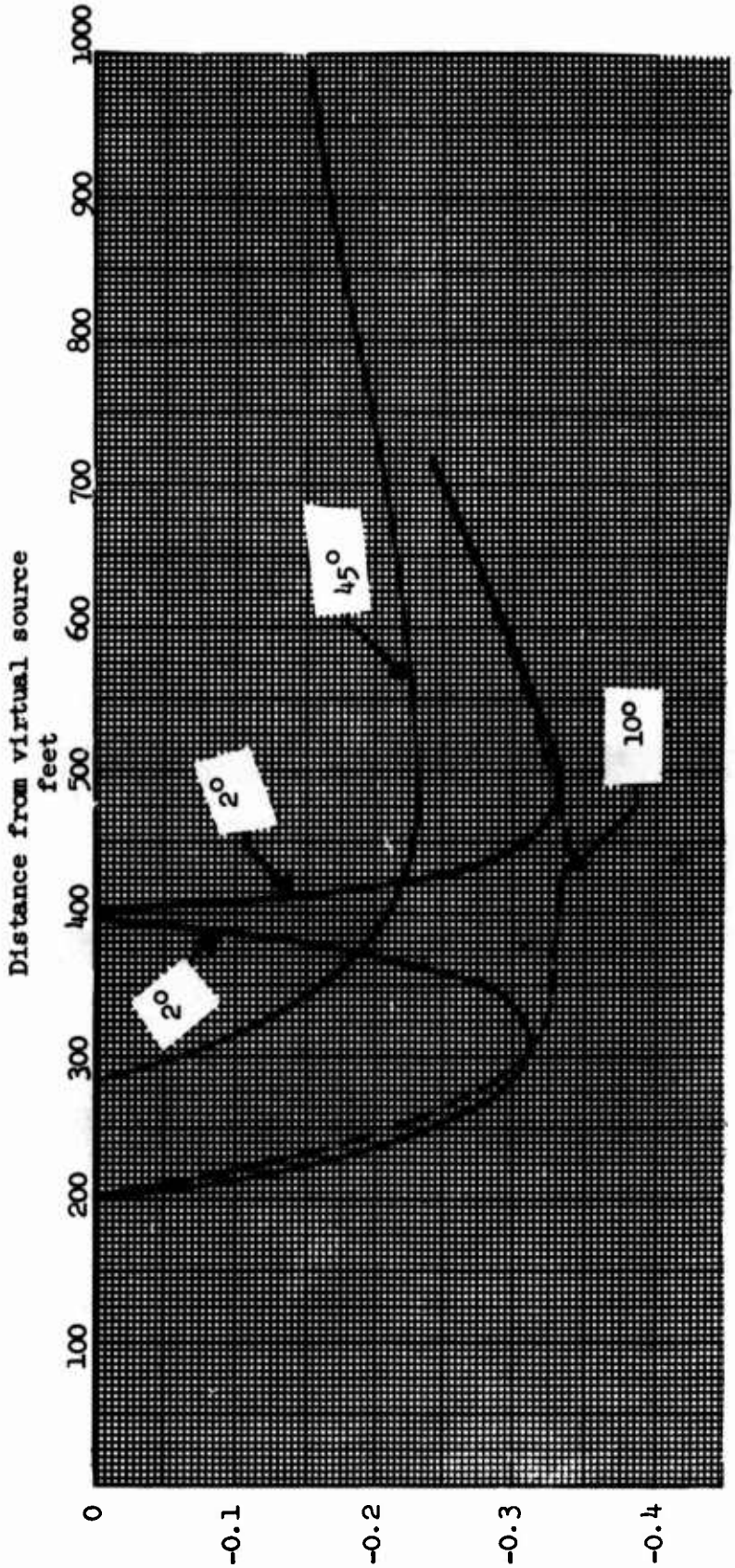

Fig. 3--Dimensionless total pressure as a function of distance from "virtual" source at time of maximum tension for angles of 2°, 10°, and 45° from the vertical. Burst depth = 200 ft.

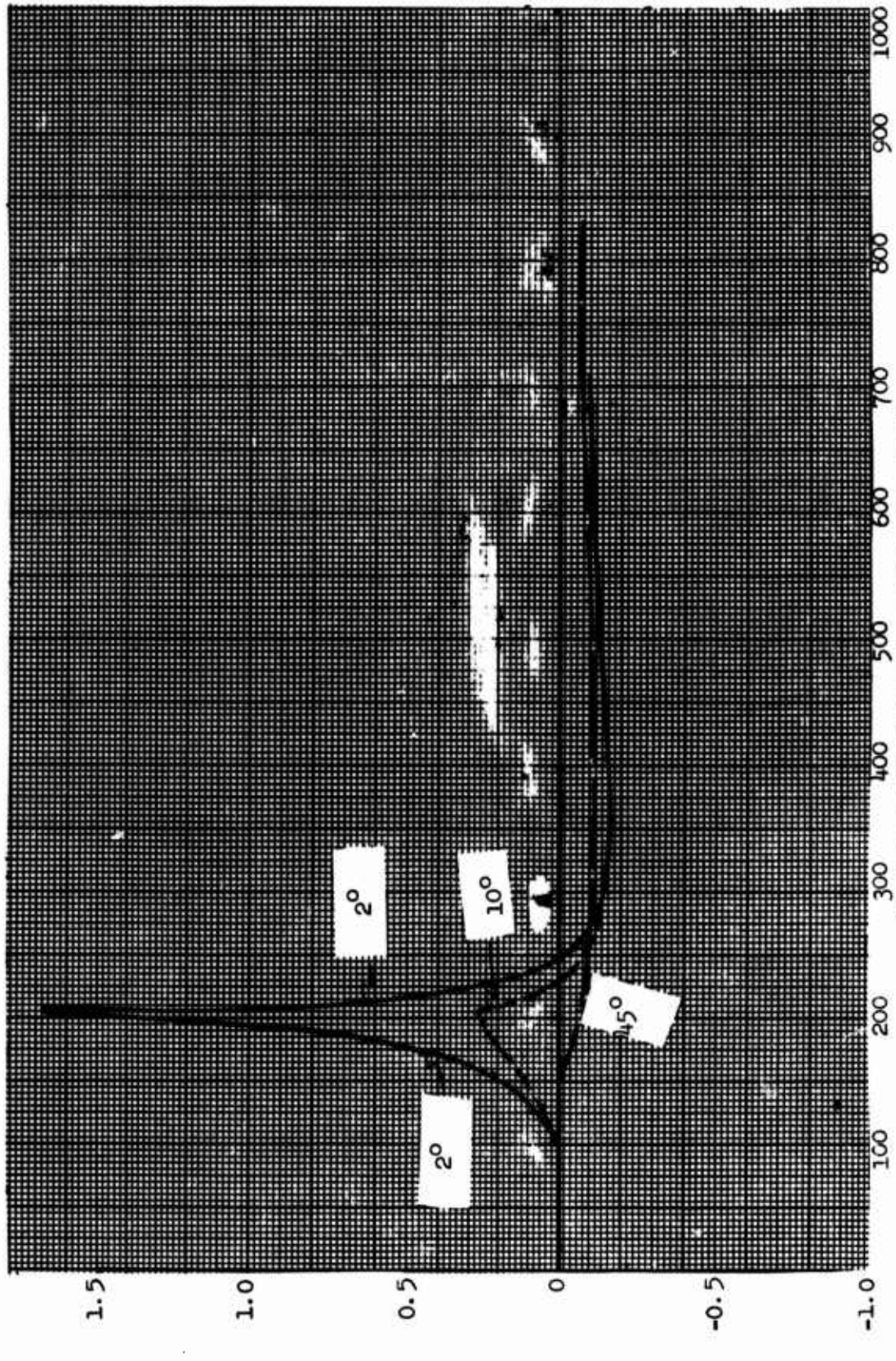

Fig. 4--Dimensionless total pressure as a function of distance from "virtual" source at time of maximum tension for angles of 2^0, 10^0, and 45^0 from the vertical. Burst depth = 100 ft.

was equal to zero at the surface was determined through a first order approximation. It was found that this condition is reached when

$$h \approx 340 \cdot d^{1/2} \quad , \qquad (21)$$

where h and d are in feet. It is rather interesting to observe that the value of h so determined is independent of the yield of the explosion although it must be remembered that this is only a first order approximation and is not valid for d > 1150 feet, approximately.

A breakdown of the total pressure into its components appeared to be of some interest, so in Fig. 5 the components of one of the curves plotted in Fig. 3 are plotted as a function of r_1. P_a is constant and has such a small value (10^{-3}) that it could not be plotted. It can be seen that the hydrostatic pressure is uniformly increasing with r_1 and the reflected rarefaction pressure is uniformly decreasing with r_1. However, as we go along a ray from the "virtual" source the pressure from the original explosion behaves very erratically and it is the variation of this pressure that produces the unusual facets in the total pressure. To look into the source of this variation it was thought to be of interest to determine the phase of the compression wave as sampled along a given ray at the head of the rarefaction wave. Phase, in this sense, is the value of the exponent, namely $r_1 - r$. Figure 6 shows $r_1 - r$ as a function of r_1 for two representative rays.

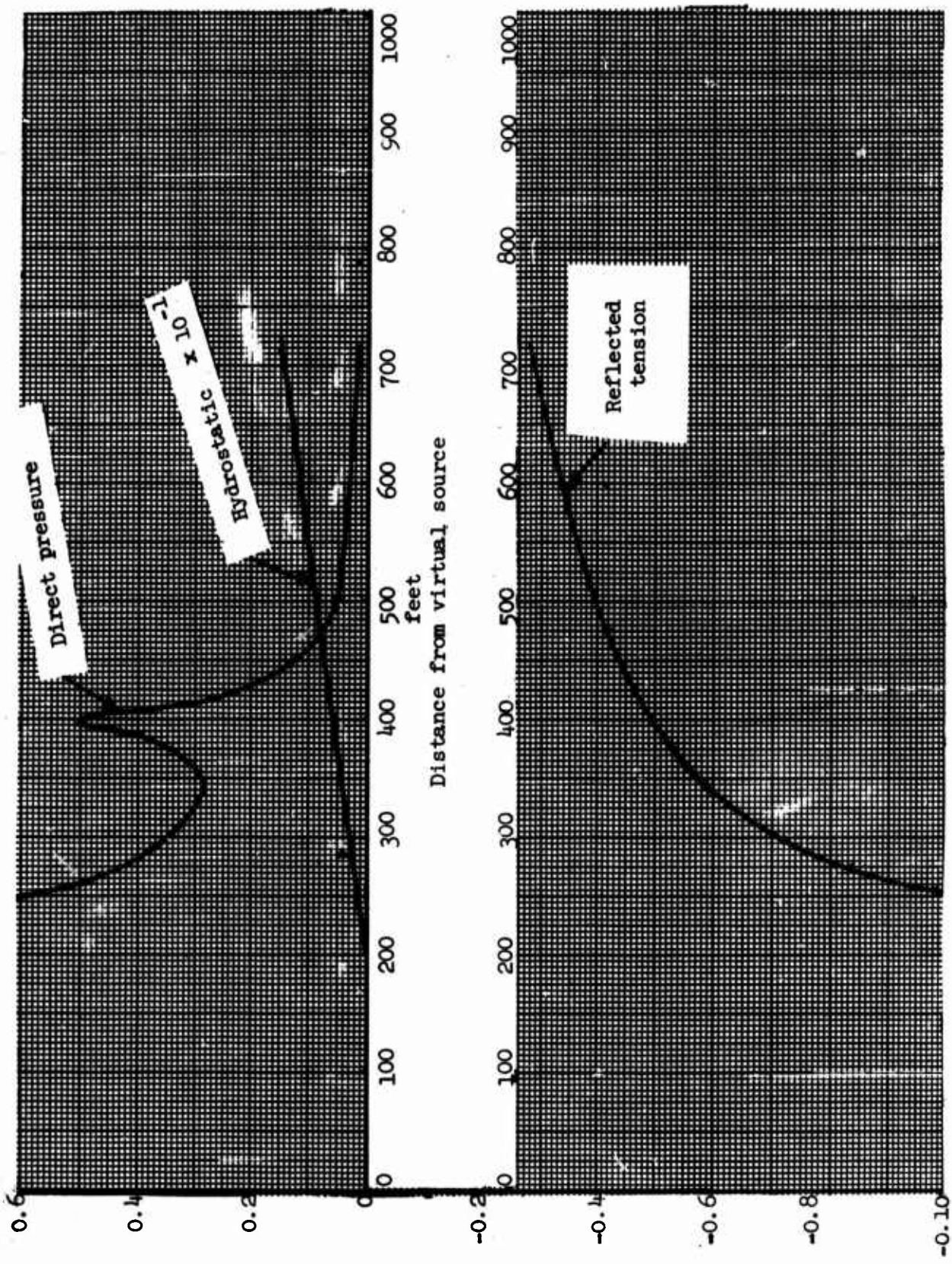

Fig. 5--Dimensionless pressure components for 2^{o} curve of Fig. 3.
Yield = 10 KT, burst depth = 200 ft.

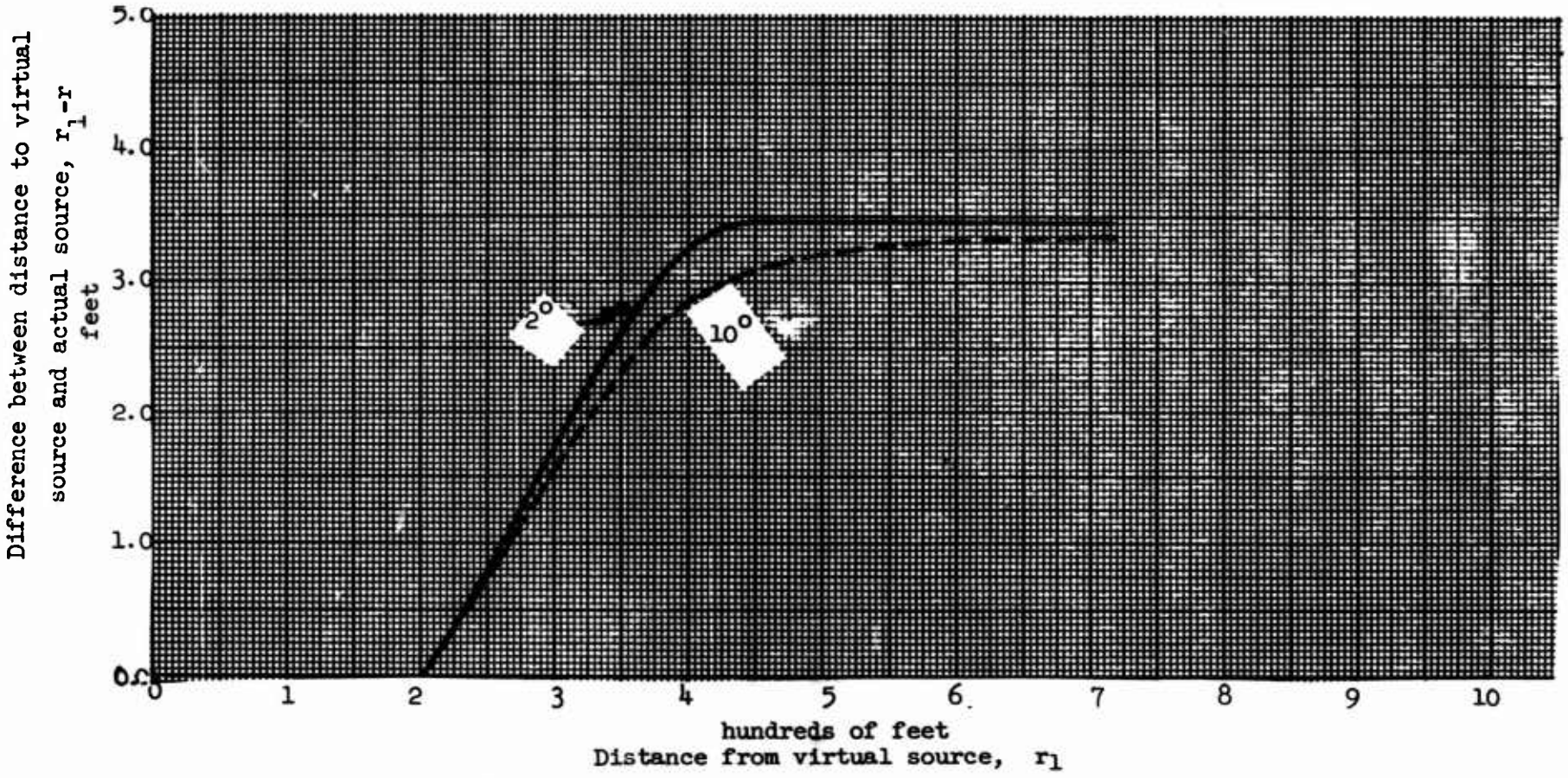

Fig. 6--"Phase" of compression wave at time of maximum tension; yield = 10 KT, burst depth = 200 ft.

IV. EXTENT OF CAVITATION

Having developed the pressure field assuming no cavitation, the next step is to determine how this pressure field is altered by cavitation. The basic criteria for the commencement and termination of cavitation were discussed in some detail in the already cited report bearing on the one-dimensional model of bulk cavitation. The same basic theory is now followed in the development of the extent of cavitation in the three-dimensional case. Cavitation will commence at any point at which the tension reaches some constant value which might be called the rupture or breaking pressure. This pressure is a function of the fluid being considered. There is considerable doubt as to what is the proper value of the breaking pressure for seawater; however, it developed in the one-dimensional case that the exact numerical value of this quantity did not strongly effect the results and so not too much attention has been paid to determining the best value of this constant. In the present study two values of this breaking pressure have been used. One is -10 psi and the other is -100 psi. It is felt that with these two values the range of practical realistic values will be represented.

It might then be thought that the cavitation or rupture process will continue until the total pressure exceeds this rupture or breaking pressure. However, a more careful analysis of the situation indicates that this is not the proper criterion for the termination of cavitation. If we consider that the rarefaction front does not have a truly instantaneous rise, then we can see that as cavitation commences the breaking front is eroded away so that the tail of the rarefaction wave is lost and that portion of the head above the tension required to maintain breaking pressure (or tension) is eroded away and not carried through the cavi-

tated region[4]. Now, cavitation is clearly a dissipative process and not a regenerative one so if at any point, the negative pressure or tension required to maintain cavitation must be increased, this increase cannot be physically realized and so cavitation must terminate. Now, in the three-dimensional case, not only is the pressure at the breaking front being attenuated by the cavitation process, but also, due to the increasing volume of the sphere as the wave moves from the center, there is an additional attenuation factor proportional to the inverse of the distance from the source. Hence in the-three dimensional case the criterion for the termination of cavitation is that the product of the distance from the virtual source, which is the point of origin of the rarefaction wave, and the minimum tension or negative pressure required to maintain rupture pressure must never increase in absolute value. Another viewpoint is that the pressure P_r at the rarefaction front, in the absence of rupture, is described in the acoustic approximation by

$$P_r = S/r_1 \tag{22}$$

where

S is the (virtual) source strength;

r_1 is distance from the virtual source.

Now with cavitation it is physically possible to reduce the effective value of S by the rupture process--but it is impossible to increase it. Hence, while cavitation is taking place we have

$$\frac{dS}{dt} = \frac{d(r_1 P_r)}{dt} < 0 \tag{23}$$

---

[4]Vincent Cushing; loc. cit. pp. 57-59.

When there is no rupture the wave travels as an acoustic wave, with spherical divergence, and with S equal to a constant, i.e.

$$\frac{dS}{dt} = \frac{d(r_1 P_r)}{dt} = 0 \qquad (24)$$

After termination of cavitation the rarefaction wave assumes a peak value equivalent to that which it had upon termination and thereafter progresses onward with the inverse distance attenuation, presumably indefinitely. However, if at any time the total pressure including this attenuation and the reduced rarefaction front reaches a value equal to the rupture pressure again, then cavitation will again commence and continue until the same criterion as used above for the termination of cavitation is again reached.

Now, a priori, it may seem unreasonable to talk of two regions of cavitation along a given ray, however, upon finding the numerical values for the extent of cavitation it was found that in some cases there was a sharp break between two adjacent points on the curve representing the termination of cavitation. Also, some of the total pressure curves presented in Section III, Figs. 2-4, indicated that the region of cavitation might be doubly-connected. A further investigation of these cases indicated that in the model used in this study, at least, it is certainly possible under some conditions to have two cavitating regions along a given ray.

Now to define these criteria mathematically we will pick up equation (20) for the total pressure at the head of the rarefaction wave

$$P_t(z,h) = d\left[\frac{e^{-(r_1 - r)}}{r} - \frac{1}{r_1}\right] + Gz + P_a \qquad (20)$$

Now, when this total pressure is equal to P_b, the breaking pressure, which it must be remembered is a negative number, cavitation will commence. Thus the criteria for the commencement of cavitation for the first time along the ray is

$$d\left[\frac{e^{-(r_1 - r)}}{r} - \frac{1}{r_1}\right] + Gz + P_a - P_b = 0 \qquad (25)$$

The negative pressure or tension required to maintain the total pressure at a point in the cavitated region at precisely the breaking pressure is given by

$$P_2 = P_b - P_a - Gz - \frac{de^{-(r_1 - r)}}{r} \qquad (26)$$

The criterion for the termination of cavitation is that the $r_1 P_2$ reach a minimum value. This must be interpreted as a minimum absolute value since P_2 is negative and hence the value of the actual product is a maximum. This condition may be expressed by the following equation

$$\frac{d(r_1 P_2)}{dr_1} = P_2 - Gr_1 \cos a - \frac{r_1}{r} de^{-(r_1 - r)} \left\{ -1 + \left[1 - \frac{1}{r}\left[\frac{r_1 - 2d \cos a}{r}\right]\right]\right\} = 0 \qquad (27)$$

where a is the angle between the ray being considered and the vertical. Now, if the value of r_1 which meets this criterion is designated r_{1s} and the value of P_2 at this value of r_1 is denoted by P_{2s}, then the total pressure in the region below this cavitated region can be represented by

$$P_t(z,h) = \frac{de^{-(r_1 - r)}}{r} - \frac{P_{2s} r_{1s}}{r_1} + Gz + P_a \qquad (28)$$

and cavitation will begin a second time whenever this total pressure becomes equal to the rupture pressure. The second cessation of cavitation will occur when the condition given by Eq. (4) is again satisfied.

A. Numerical Results

Using the model described above, a series of numerical results have been obtained for various explosions in which both the depth of burst and the explosive yield have been varied. In order to obtain these numerical results certain pressures had to be evaluated. These explosive parameters were based on the results of previous tests. The following parameters were used:

$P_a = 14.7$ psi

$G = 64.4$ lbs/cu. ft.

$P_s = 1.38 \times 10^6 W^{1/3}/d$ psi

$\lambda = 53.5 W^{1/3}$ ft.

where W is the yield of the explosion in kilotons

d is the depth of the explosion in feet.

Using these constants the results shown in Figs. 7 through 24 were obtained for the extent of the cavitated region under the conditions noted on each figure. In Table 1 the various conditions shown in the figures are listed together with some of the results.

It can be seen that there are four types of explosions from a cavitation viewpoint. There is one type in which the cavitated region is singly connected and above the explosion in the immediate neighborhood of the explosion. Two, there is the type of explosion in which the cavitated region is doubly connected and a non-cavitated "ball" exists around the explosion. Three, the case in which the cavitated region is singly connected and is completely below the explosion in the immediate region of the burst point. Lastly, if the explosion occurs at great depth, there will be no cavitation at all. A further study was made to determine approximately the boundaries between these four regions and it was found that a

TABLE I.

TYPES OF EXPLOSIONS INVESTIGATED

Case	Yield -KT	Burst Depth - ft.	Breaking Pressure - psi	Type of* Cavitation	Maximum Horizontal Extent of Cavitation - ft.	Maximum Depth of Cavitation - ft.	Illustrated in Figure No.
1	10	200	-10	2	3,360	460	7
2	10	200	-100	2	2,400	445	8
3	1	1000	-100	1	4,830	140	9
4	1	1000	-10	1	7,500	190	10
5	1	200	-100	1	2,280	230	11
6	1	200	-10	1	3,230	240	12
7	10	1000	-10	1	8,210	310	13
8	10	1000	-100	1	6,120	300	14
9	10	150	-10	2	2,800	500	15
10	13	700	-10	1	6,900	430	16
11	20	70	-10	3	1,710	680	17
12	20	150	-10	2	2,790	620	18
13	50	5000	-10	1	17,900	380	19
14	20	5000	-10	1	17,100	300	20

*Type 1 - Region of cavitation above burst depth in vertical plane of explosion.

Type 2 - Region of cavitation both above and below burst depth in vertical plane of explosion.

Type 3 - Region of cavitation below burst depth in vertical plane of explosion.

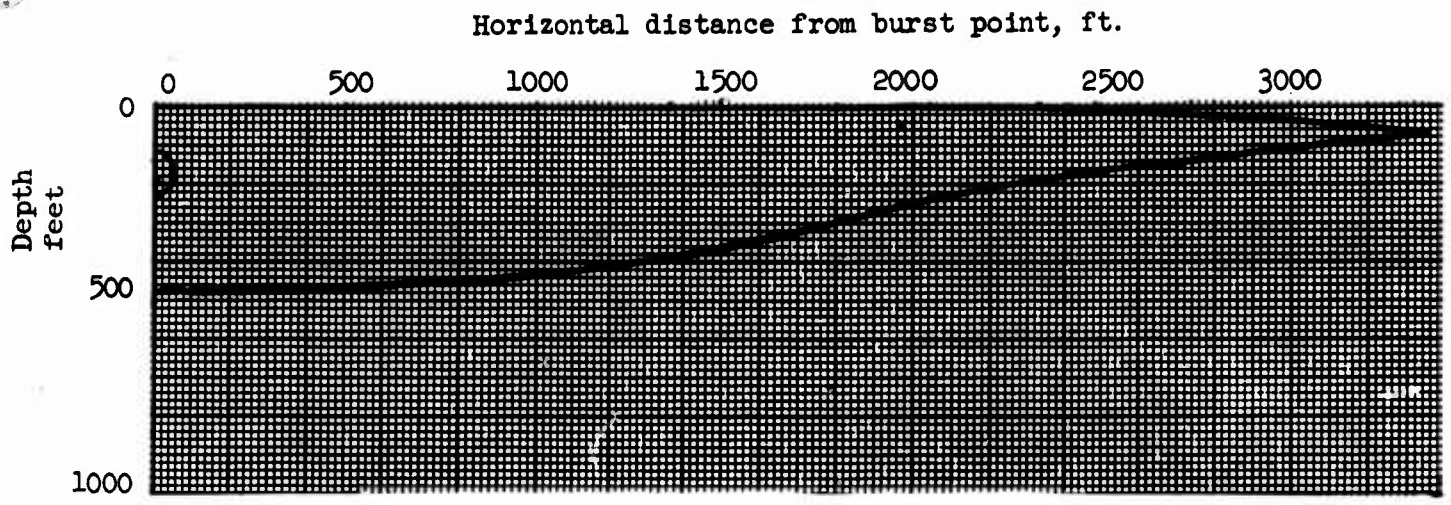

Fig. 7a--Extent of cavitated region; yield = 10 KT, burst depth = 200 ft., rupture pressure = -10 psi.

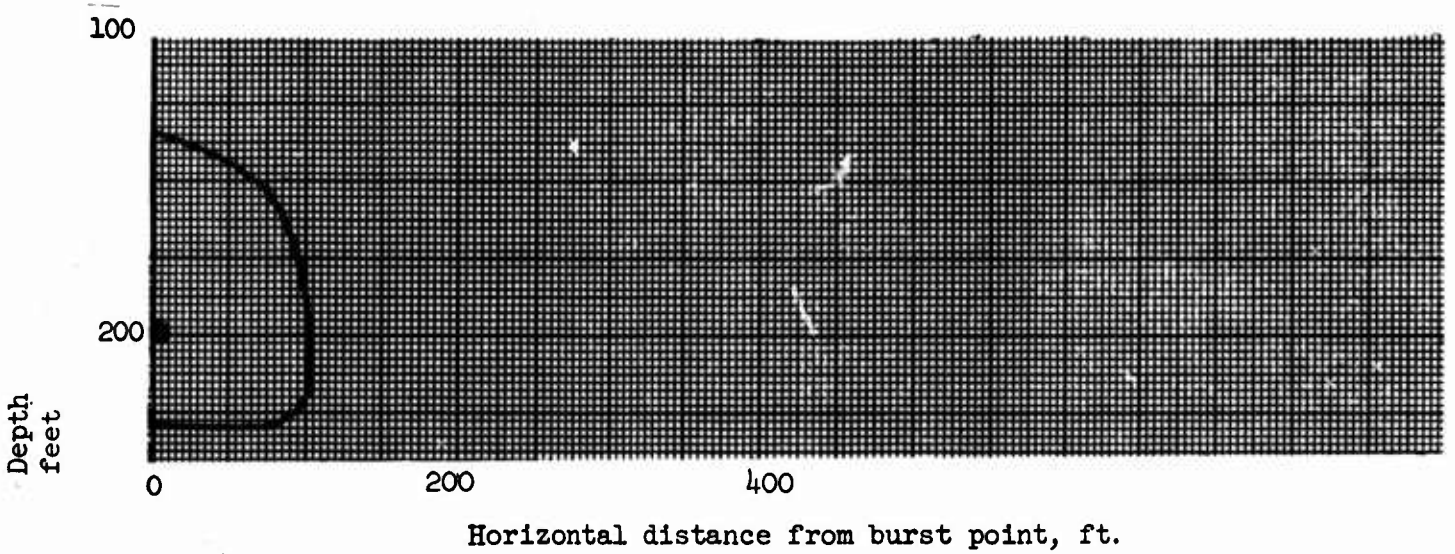

Fig. 7b--Detail of area around burst point.

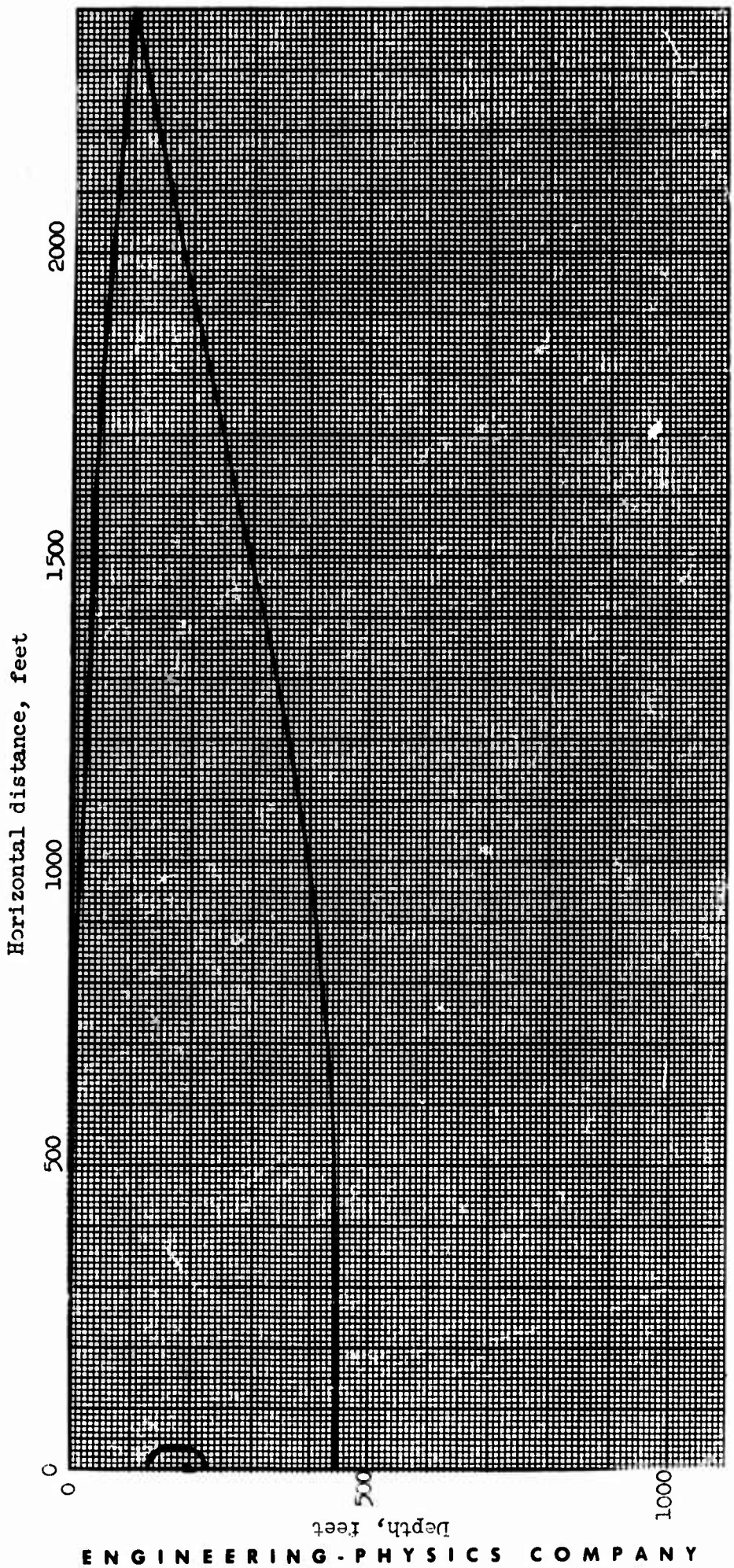

Fig. 8--Extent of cavitated region; yield = 10 KT,
burst depth = 200 ft., rupture pressure = -100 psi.

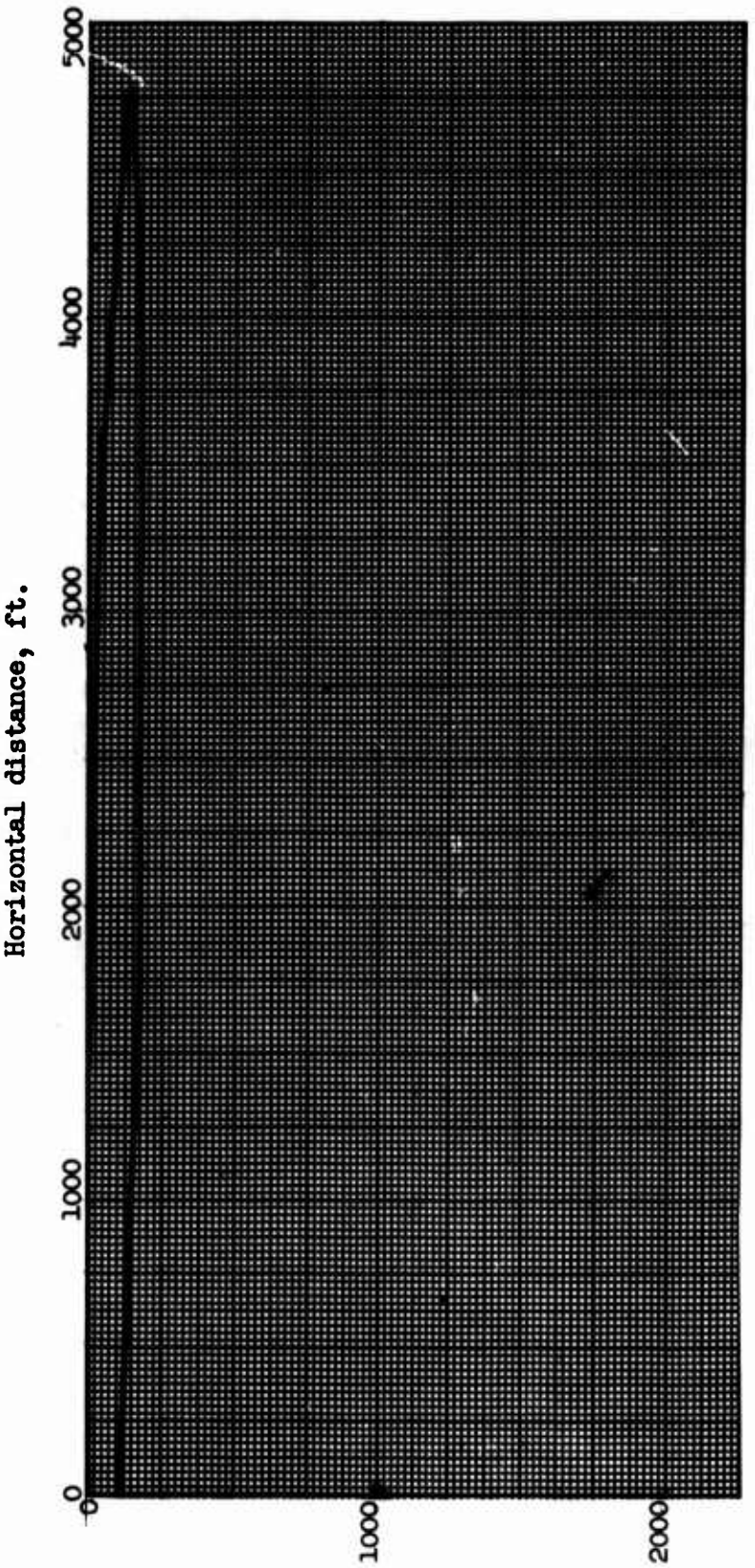

Fig. 9--Extent of cavitated region; yield = 1 KT,
burst depth = 1000 ft., rupture pressure = -100 psi.

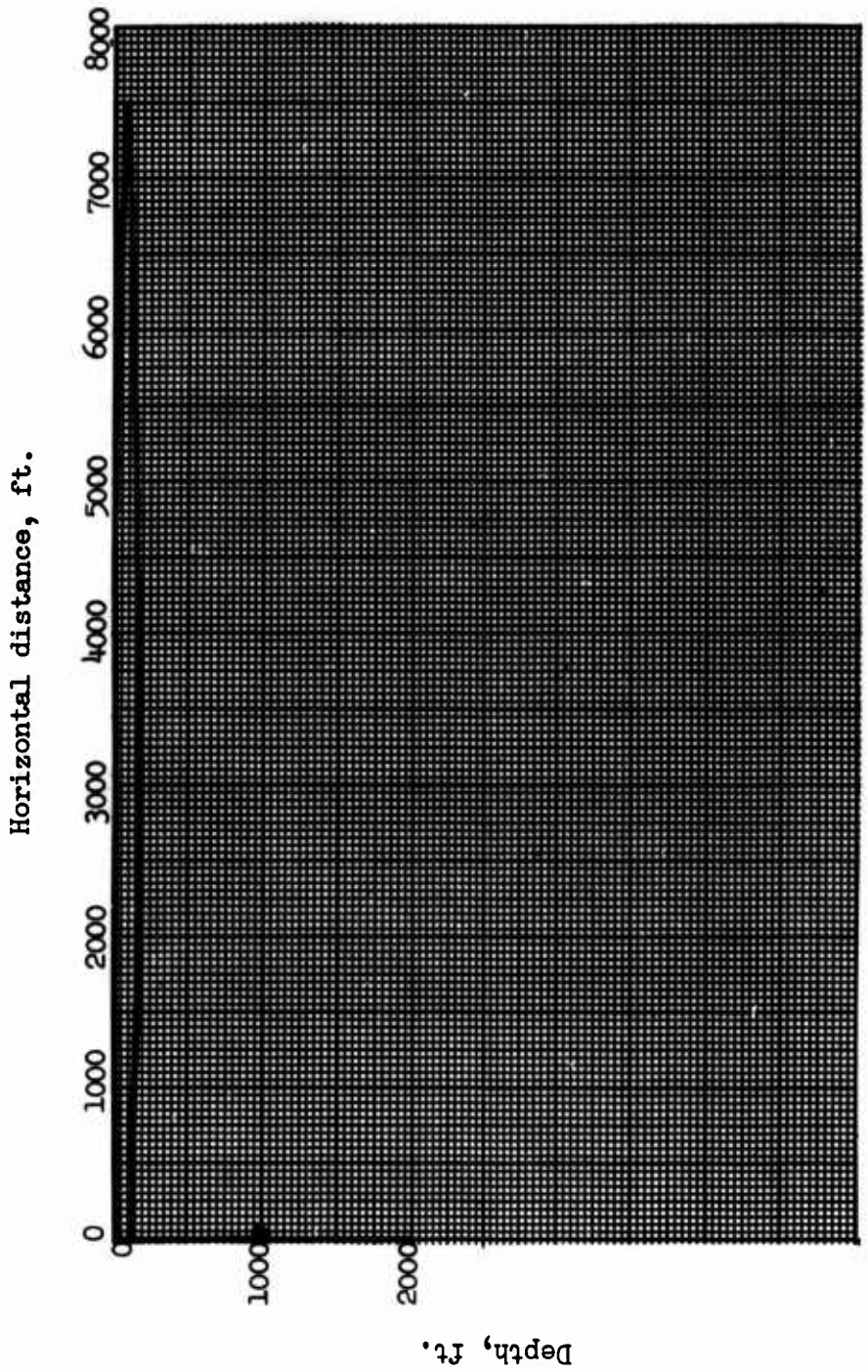

Fig. 10--Extent of cavitated region; yield = 1 KT;
burst depth = 1000 ft., rupture pressure = -10 psi.

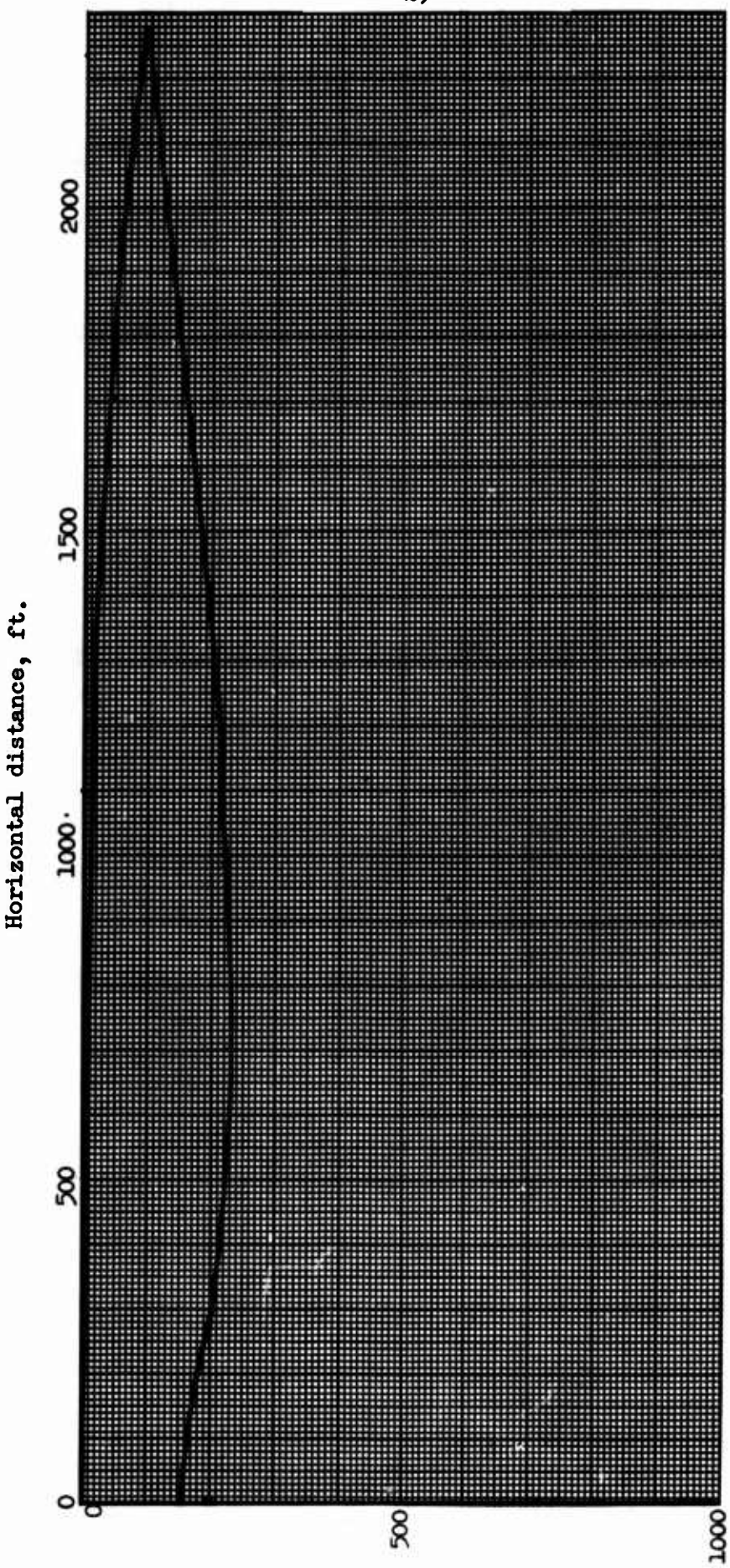

Fig. 11--Extent of cavitated region; yield = 1 KT, burst depth = 200 ft., rupture pressure = -100 psi.

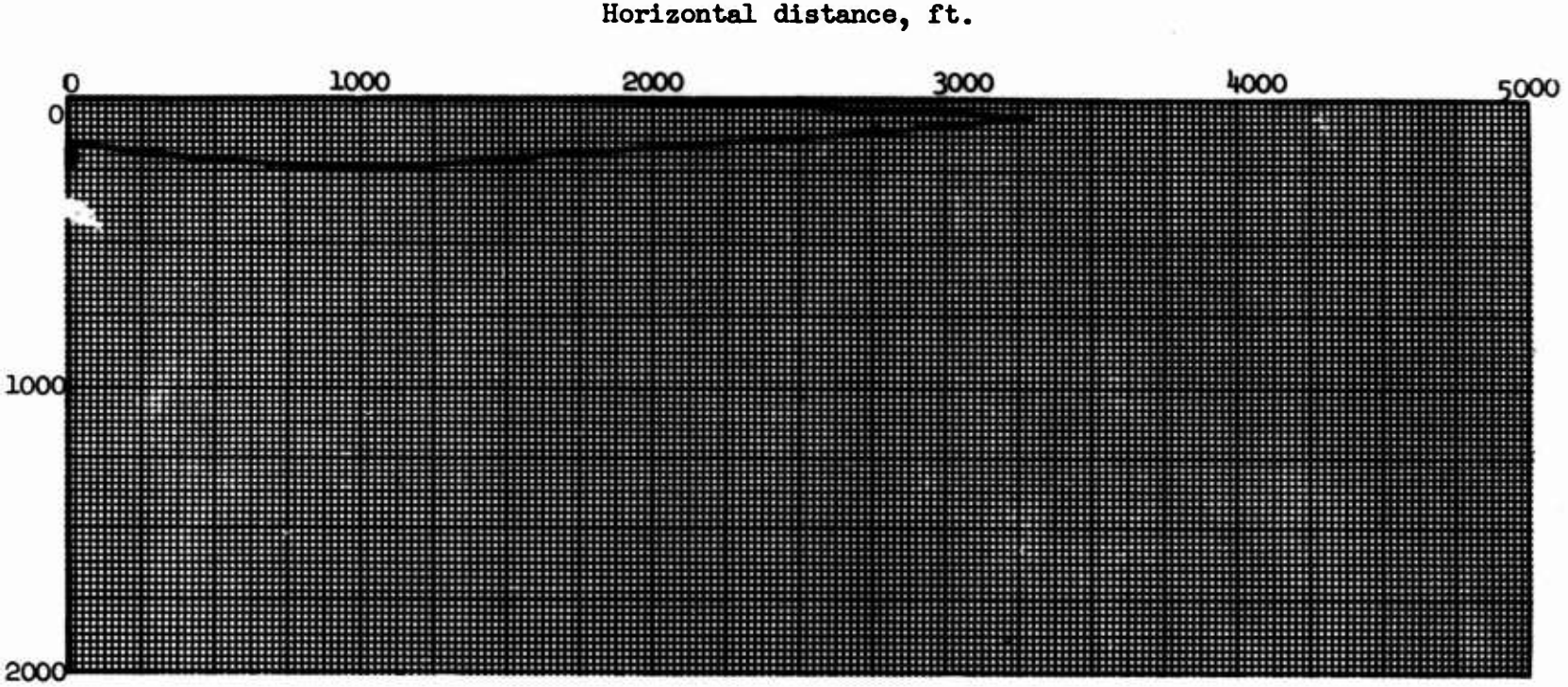

Fig. 12--Extent of cavitated region; yield = 1 KT,
burst depth = 200 ft., rupture pressure = -10 psi.

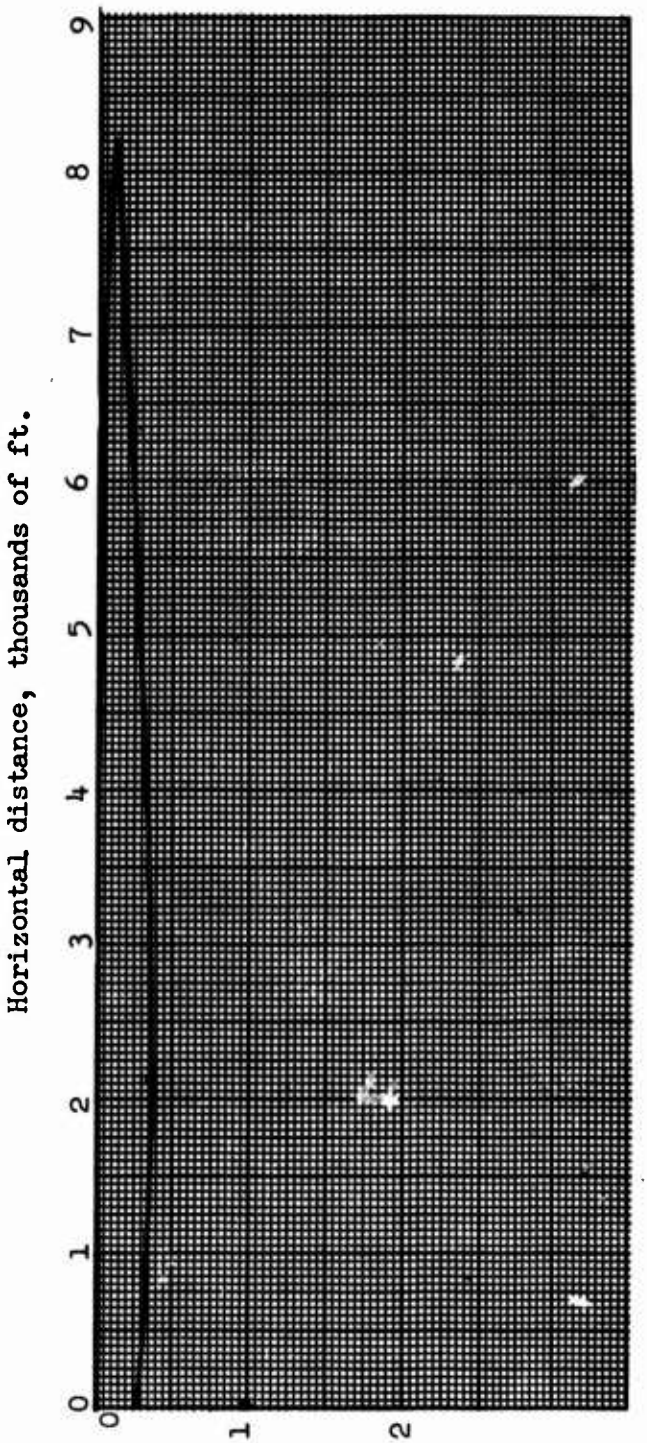

Fig. 13--Extent of cavitated region; yield = 10 KT,
burst depth = 1000 ft., rupture pressure = -10 psi.

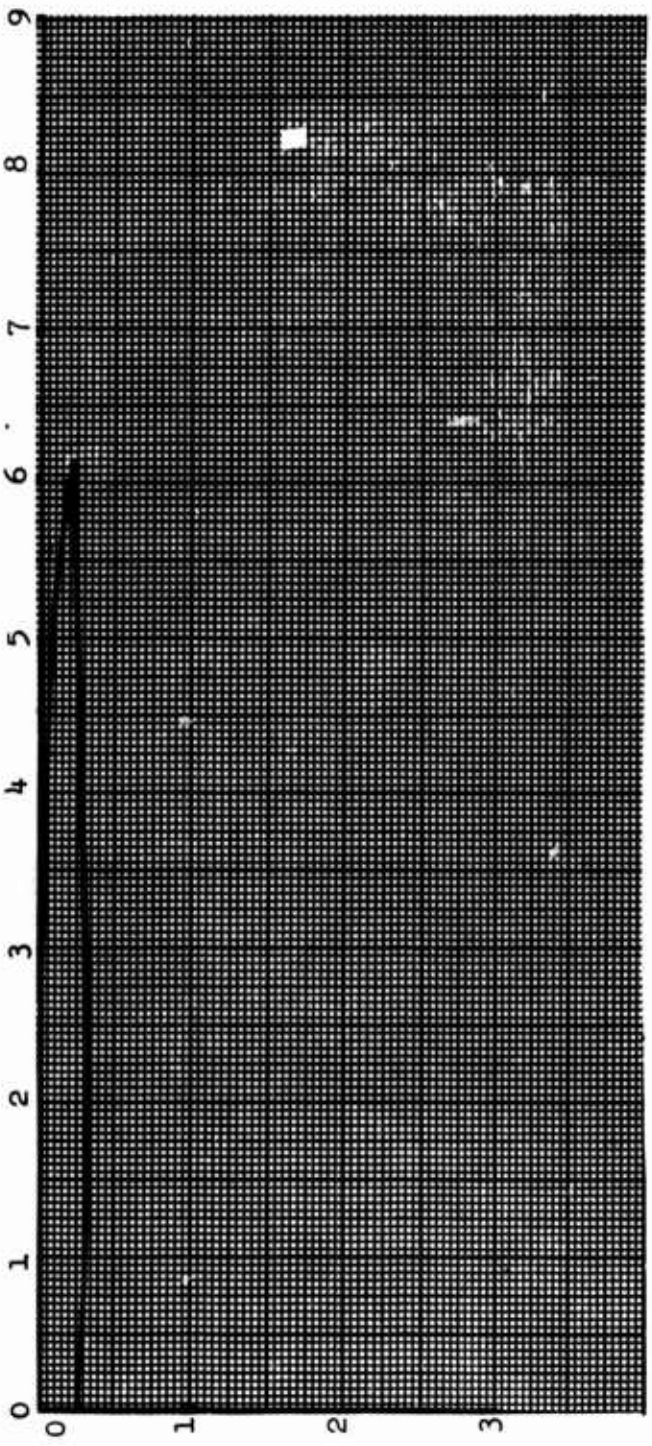

Fig. 14--Extent of cavitated region; yield = 10 KT,
burst depth = 1000 ft., rupture pressure = -100 psi.

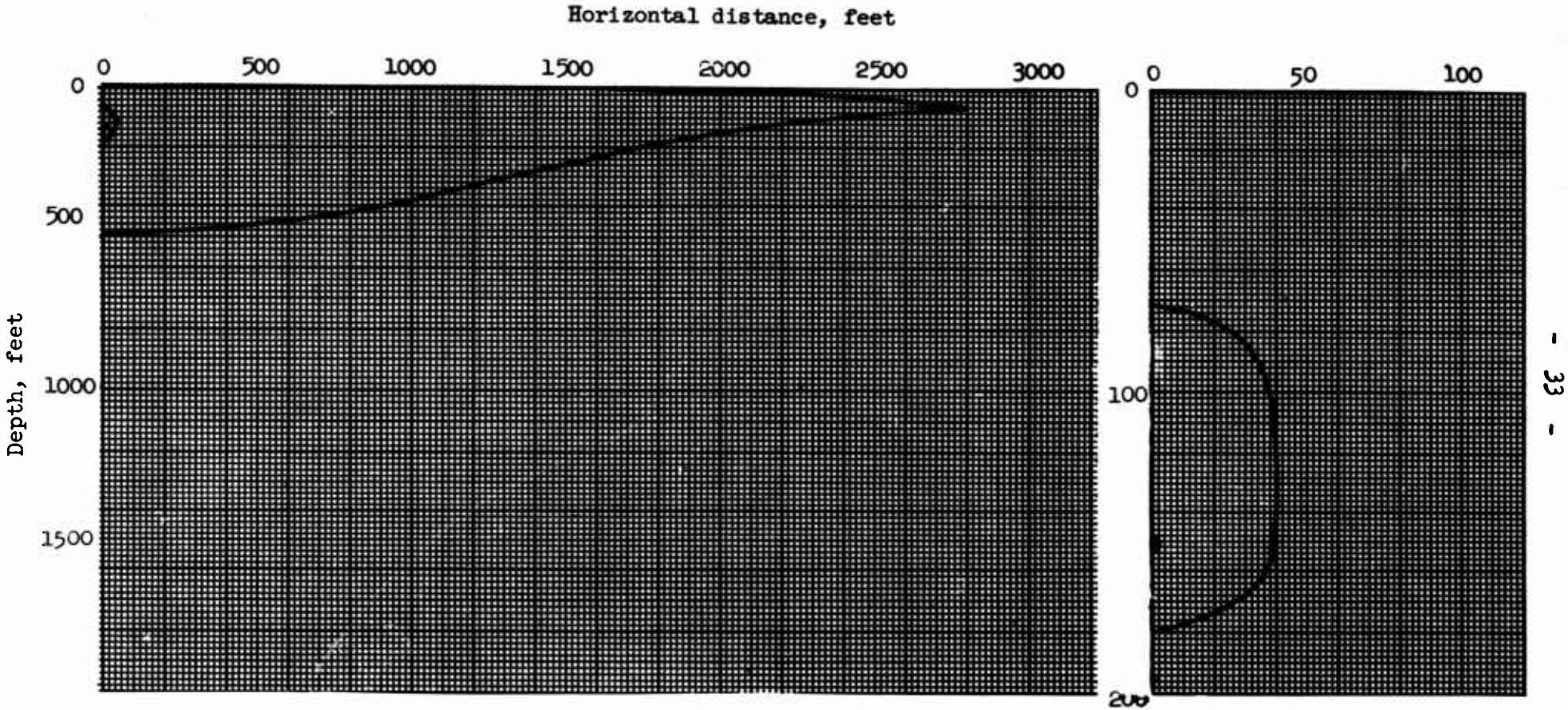

Fig. 15--Extent of cavitated region; yield = 10 KT, burst depth = 150 ft., rupture pressure = -10 psi.

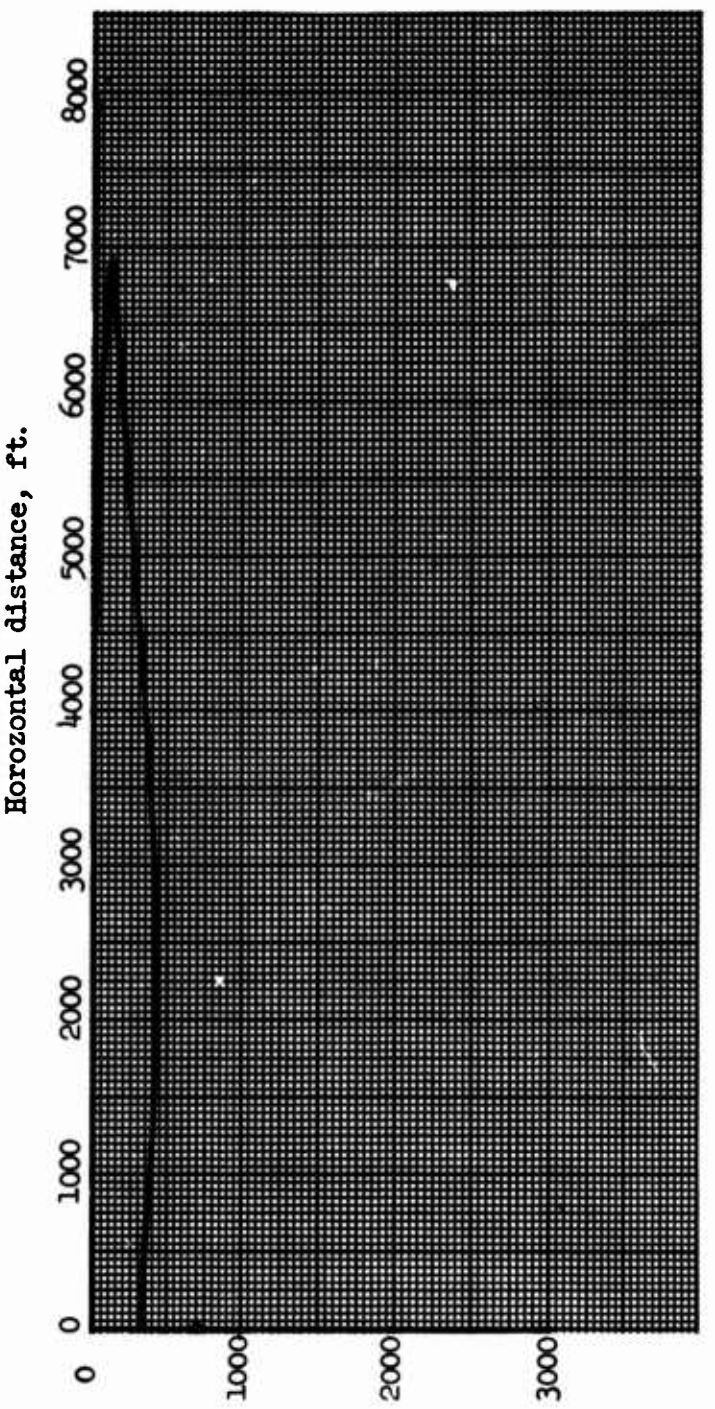

Fig. 16--Extent of cavitated region; yield = 13 KT,
burst depth = 700 ft., rupture pressure = -10 psi.

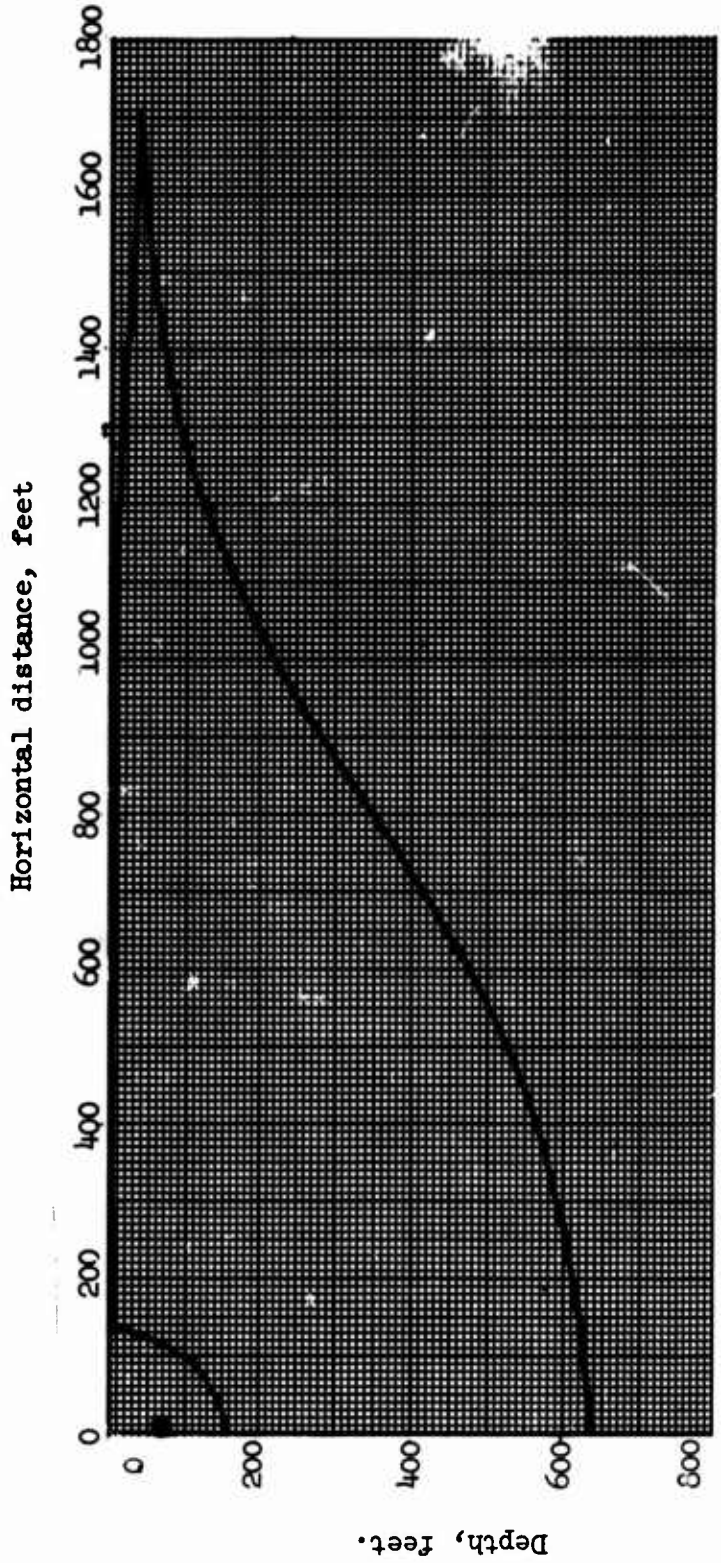

Fig. 17--Extent of cavitated region; yield = 20 KT,
burst depth = 70 ft., rupture pressure = -10 psi.

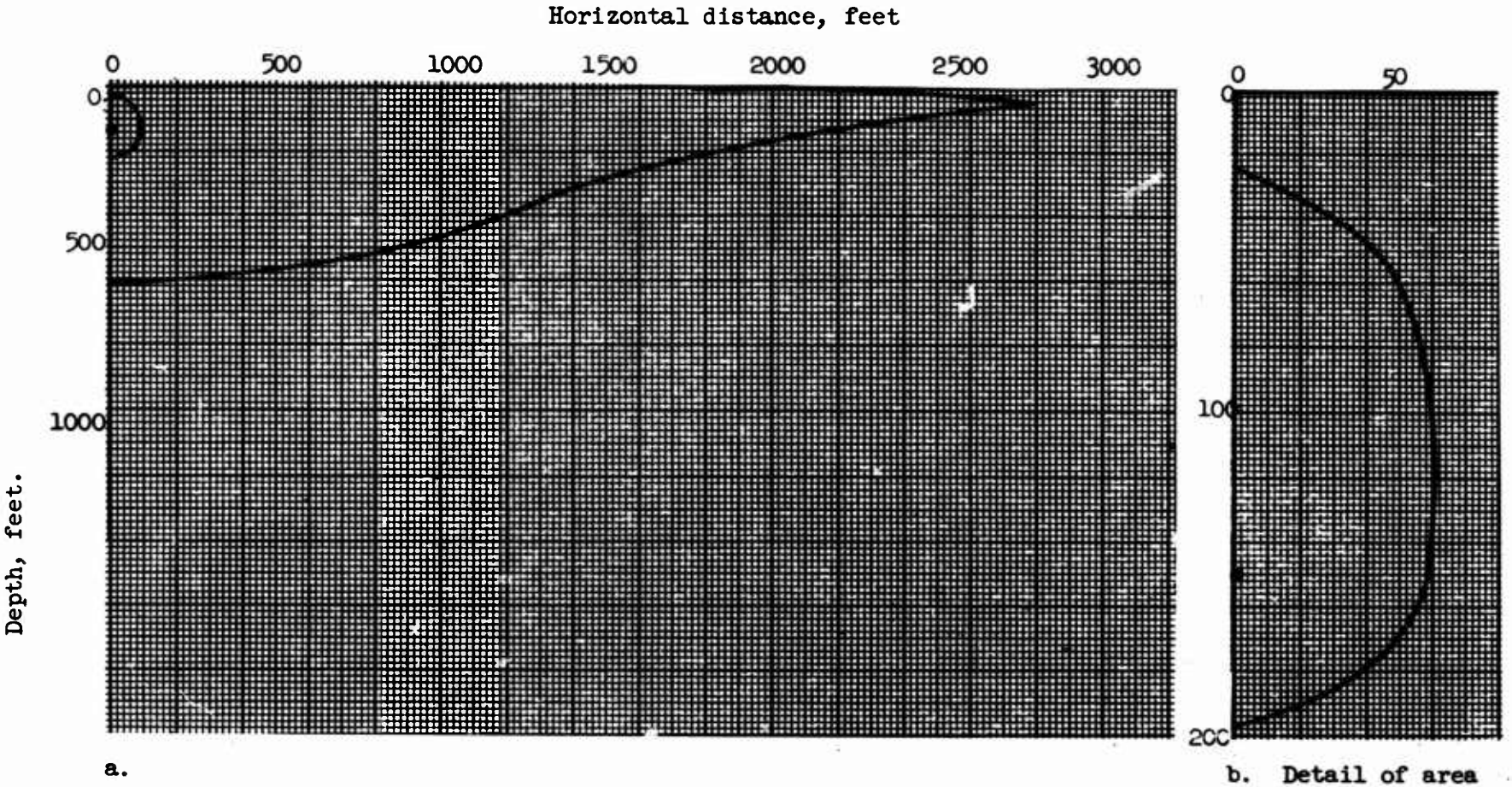

Fig. 18--Extent of cavitated region; yield = 20 KT, burst depth = 150 ft., rupture pressure = -10 psi.

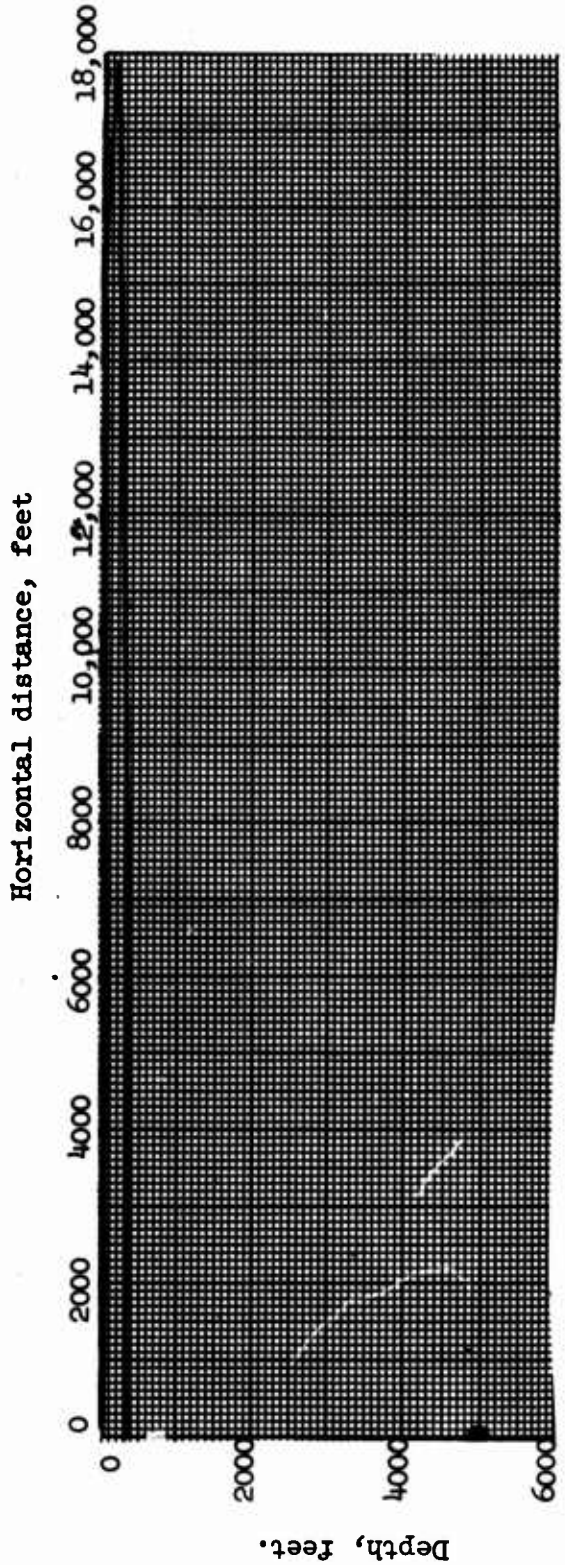

Fig. 19--Extent of cavitated region; yield = 50 MT,
burst depth = 5000 ft., rupture pressure = -10 psi.

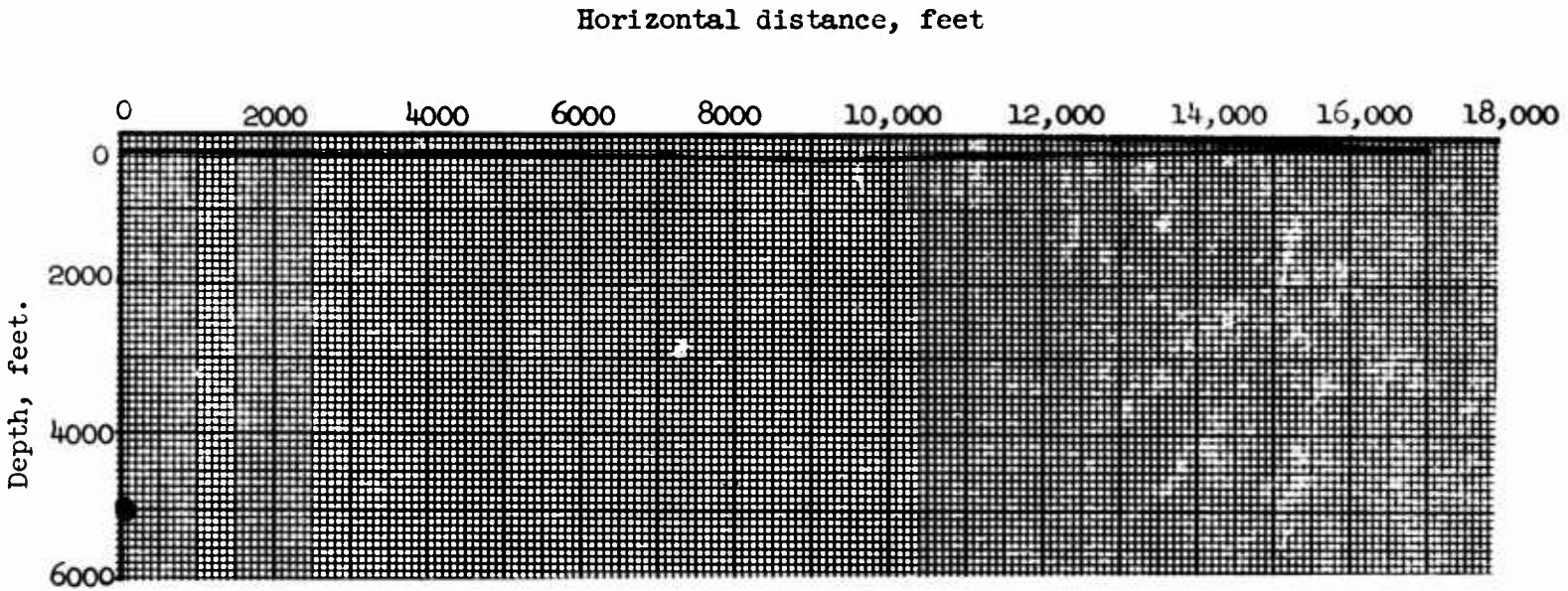

Fig. 20--Extent of cavitated region; yield = 20 KT;
burst depth = 5000 ft., rupture pressure = -10 psi.

very shallow explosion produces the third type of cavitation, namely, where all the cavitation is directly below the explosion in the region of the explosion. If the depth of the explosion is less than the value of λ, as defined above, this type of cavitation may be expected. If the depth is greater than λ but somewhat less than another value dependent to some extent upon the yield; then the doubly connected cavitated region occurs. The largest value of depth for which this condition will hold is plotted in Fig. 21 as a function of yield. Fig. 22 shows a plot of the dimensionless depth (d/λ) which forms this boundary as a function of yield. If the explosion takes place at a depth greater than that indicated in Fig. 21, the cavitated region will not extend below the burst point. If an explosion occurs at an extremely great depth, it is clear heuristically that no cavitation would exist because the negative pressures or tensions in the rarefaction wave would never be great enough to produce a net tension at any point. The exact burst depth at which the existence of a cavitated region would cease has not as yet been rigorously determined. However, it appears from preliminary results that, if P_s, the pressure due to the compression wave at the surface directly above the burst point, is less than about twice the atmospheric pressure, then there will be no cavitated region.

B. Discussion of Results

It is certainly recognized that there is no experimental evidence to support the finding of cavitation below the burst point of the explosion and, as a matter of fact, in reality it is not precisely expected that cavitation would exist directly below the burst point because the rarefaction wave, used in our model, would not be transmitted in a linear fashion through the gas bubble. However, there is a definite possibility that there may be nearly a doubly connected region of cavitation and that these results will furnish an indication of the phenomena

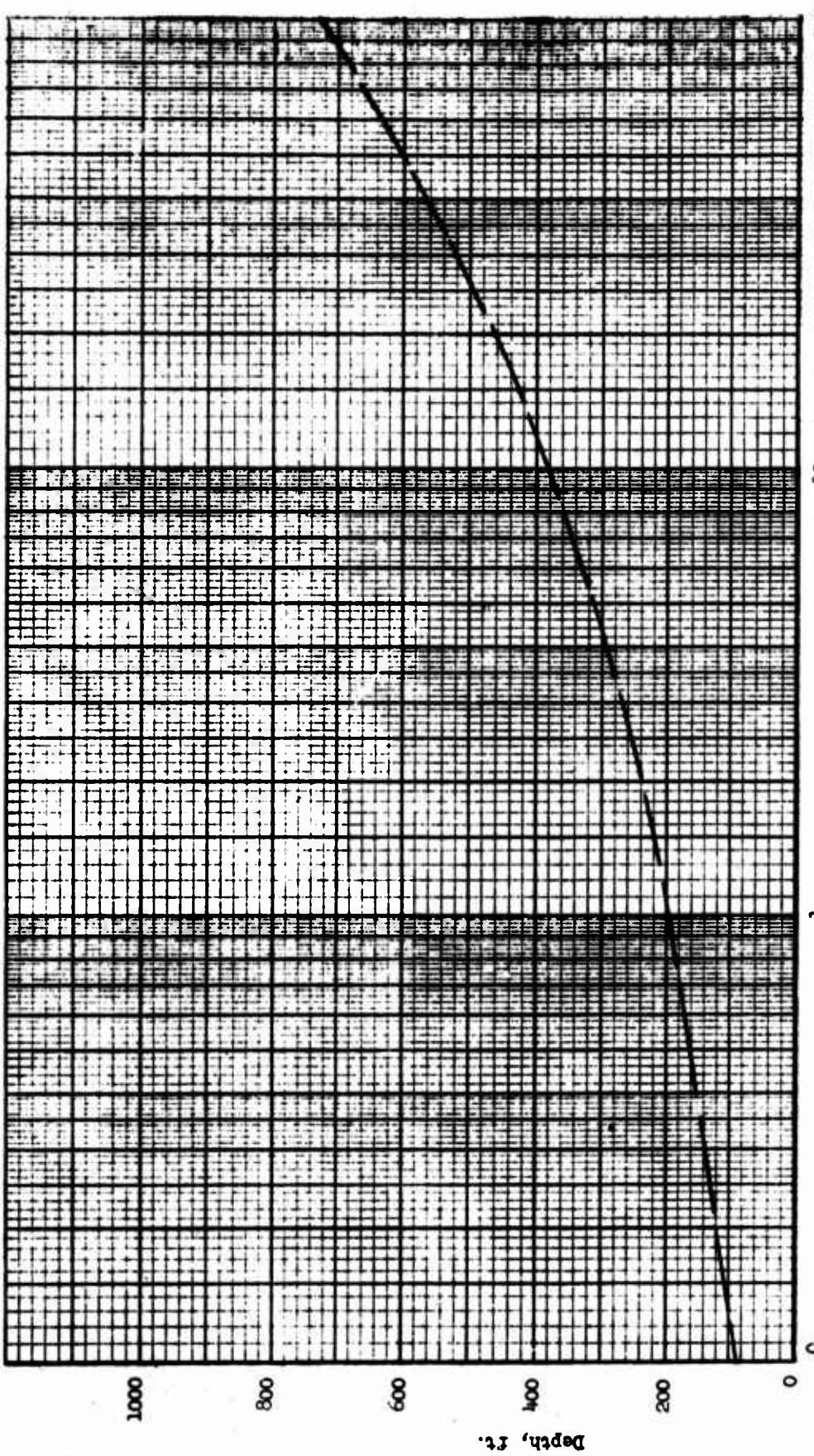

Fig. 21--Depth at which cavitation directly beneath burst point ceases as a function of yield.

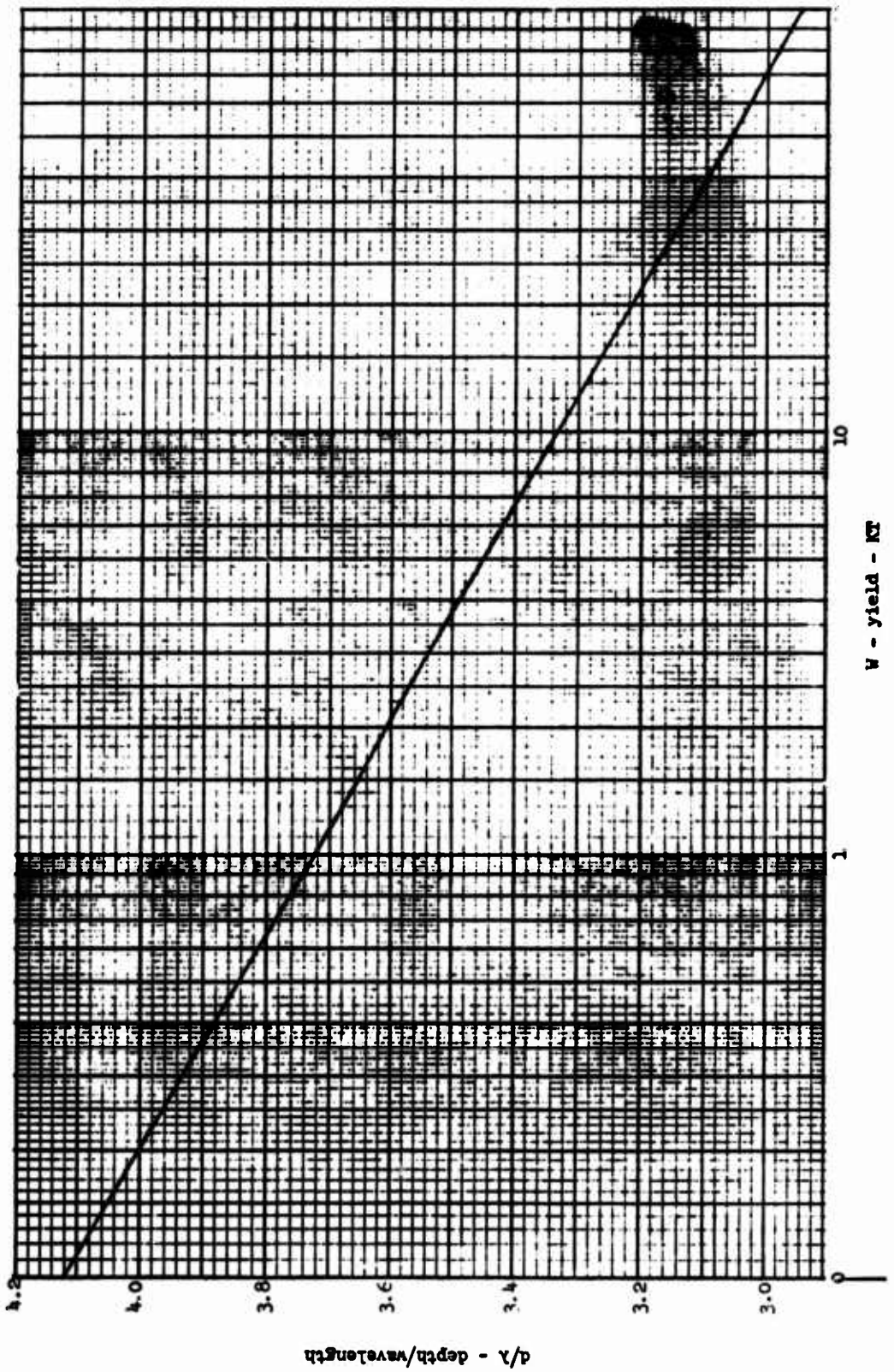

Fig. 22--Dimensionless depth at which cavitation directly beneath burst point ceases as a function of yield.

which exist under real conditions. In the very shallow explosion it may be expected that there would be an annular region of cavitation with a central region in which there was no cavitation, then a cavitating ring, and then, of course, no cavitation at great distance. In any event, it is felt that the cavitated regions below an explosion will close very quickly since the bottom surface is rigidly held and will not move downward in a way comparable to the upward movement of a slug of water when cavitation occurs above an explosion.

V. TRAJECTORY OF WATER HAMMER

The following mathematical model was developed to obtain an initial understanding of the way in which cavitation pulses are generated. For the purposes of this first study it is assumed that the layer of water overlying the cavitated region is spalled upward with an initial velocity equal to twice the vertical component of the instantaneous particle velocity associated with the pressure at the front of the shock wave. The time at which spalling takes place at any given horizontal range from the explosive source is determined from the sound speed of water and the depth of the explosion. It is further assumed that this liquid layer is acted upon only by forces due to the acceleration of gravity and furthermore that the usual acoustic relationship between pressure and particle velocity holds. In addition it is assumed that spherical divergence, $1/R$, is the only mechanism by which the magnitude of the shock wave is reduced with distance from the explosive source. It was found that this very simple model predicts a cavitation pulse of striking likeness to those observed experimentally.

In setting up the equations for the above-described model, the time required for the shock to reach a given horizontal range, h, when exploded at a depth, d, and where the shock propagates at a velocity, C, is given by

$$t = R/C \quad , \qquad (29)$$

where $R^2 = h^2 + d^2$. The time required for the liquid layer to go through its trajectory and impact with the underlying water is given by

$$\tau = 2u/g \quad , \qquad (30)$$

where u is the initial velocity of the liquid layer;

g is the acceleration of gravity.

Hence the total time required from detonation to water hammer impact is given by

$$T = R/C + 4u_v/g \quad , \qquad (31)$$

where u_v is the vertical component of particle velocity associated with the instantaneous pressure at the shock front at a horizontal distance, h, on the surface. Using the acoustic approximation, Eq. (31) can be written as

$$T = R/C + 4Pd/g\rho CR \quad , \qquad (32)$$

where ρ is the density and P is the peak pressure. We assume that the peak pressure at slant range, R, is given by

$$P = KW^{1/3}/R \quad , \qquad (33)$$

where W is the yield in kilotons;

K is a constant having a value of roughly 2×10^6 when P is in lb/in^2 and R is in feet.

Substituting Eq. (33) into Eq. (32) we obtain

$$T = R/C + 4KdW^{1/3}/g\rho CR^2 \quad . \qquad (34)$$

By differentiating Eq. (34) with respect to h and taking the reciprocal of both sides, we obtain an expression for the horizontal velocity of the traveling hammer,

$$V = \rho CgR^4/[h(\rho gR^3 - 8KdW^{1/3})] \quad . \qquad (35)$$

For increasing h and, hence, increasing R, for fixed d, it is easy to see from Eq. (35) that the water hammer velocity approaches the sound speed of water. From Eq. (35) we can also determine the horizontal distance at which first impact occurs.

$$h = [(8KW^{1/3}d/\rho g)^{2/3} - d^2]^{1/2} \qquad \text{for } d \leq (8KW^{1/3}/\rho g)^{1/2}$$

$$H = 0 \qquad \text{for } d > (8KW^{1/3}/\rho g)^{1/2} \quad . \tag{36}$$

Figure 23 shows the horizontal distance to the circle of first impact as a function of the depth of burst. From Eq. (36) we see that depending upon the depth of blast and size of the bomb the water hammer travels inward toward the source of the explosion or outward away from it or simultaneously in both directions from the circle of first impact. It is also perhaps interesting that there exists a depth of burst for a given yield which maximizes the distance to the point of first impact. This depth obtained from Eq. (36) is

$$d^* = (4/3)^{3/4}(K/\rho g)^{1/2} W^{1/6} \quad , \tag{37}$$

and the corresponding maximum first impact point can be determined by substitution of Eq. (37) into Eq. (36), to be $h = \sqrt{2}d^*$. A table giving horizontal distance of first impact and time of first impact for a few representative cases is given below.

TABLE II.

Depth Feet	Equivalent Weight - KT	Horizontal Range of First Impact - ft.	Time of First Impact - sec.
70	20.	1700	0.50
200	1.	1690	0.51
200	10.	2190	0.66
1000	1.	2740	0.87
1000	10.	3620	1.12
5000	20.	4800	2.08

Using the above equations a number of computer runs were made on an IBM 1620 to determine the water hammer trajectory. Figures 24 and 25 show typical plots of time of impact and impact velocity versus horizontal distance.

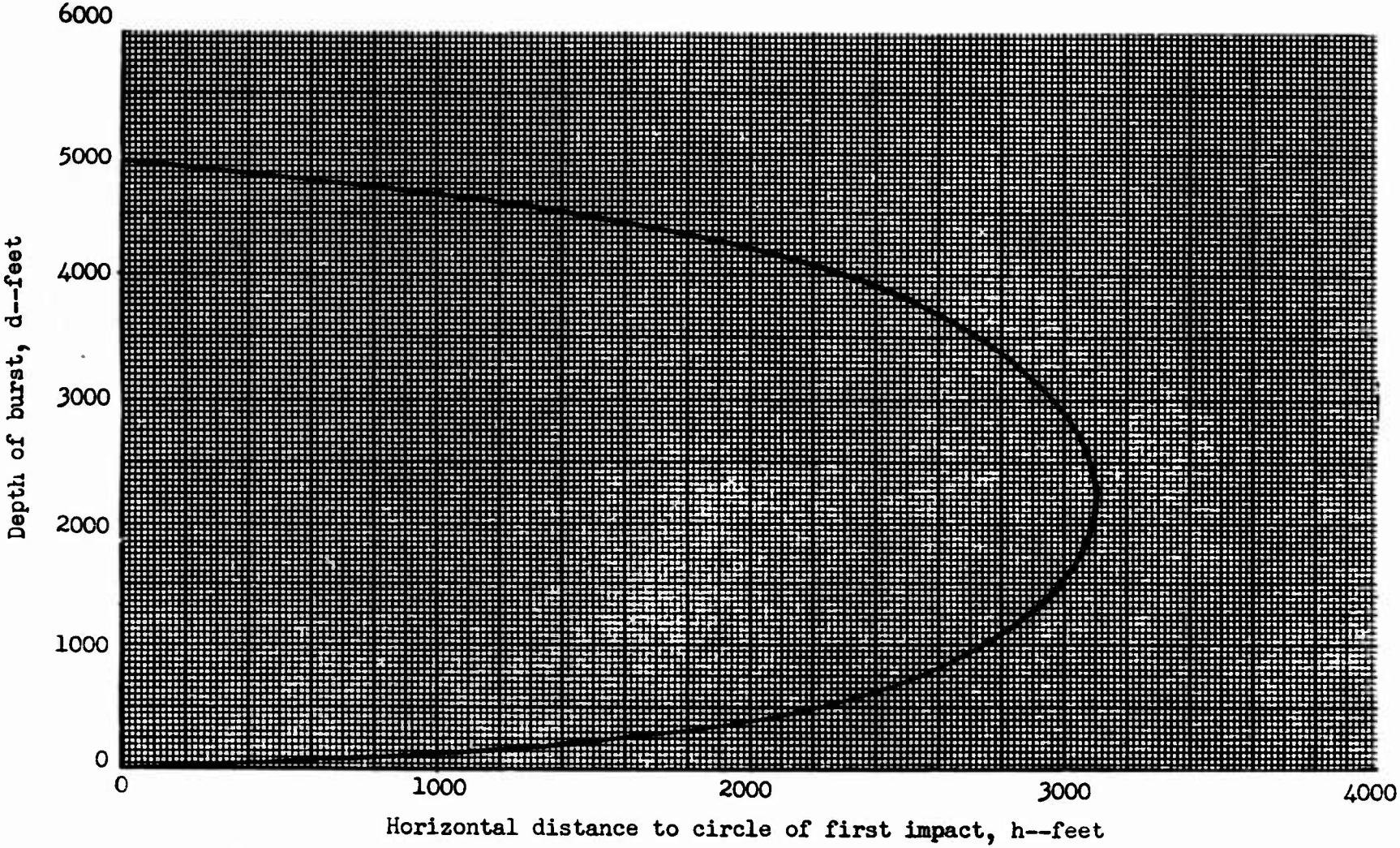

Fig. 23--Depth of burst versus horizontal distance to circle of first impact for a yield of 1 KT. First impact occurs at a point under surface zero for depth of burst greater than 4970 feet.

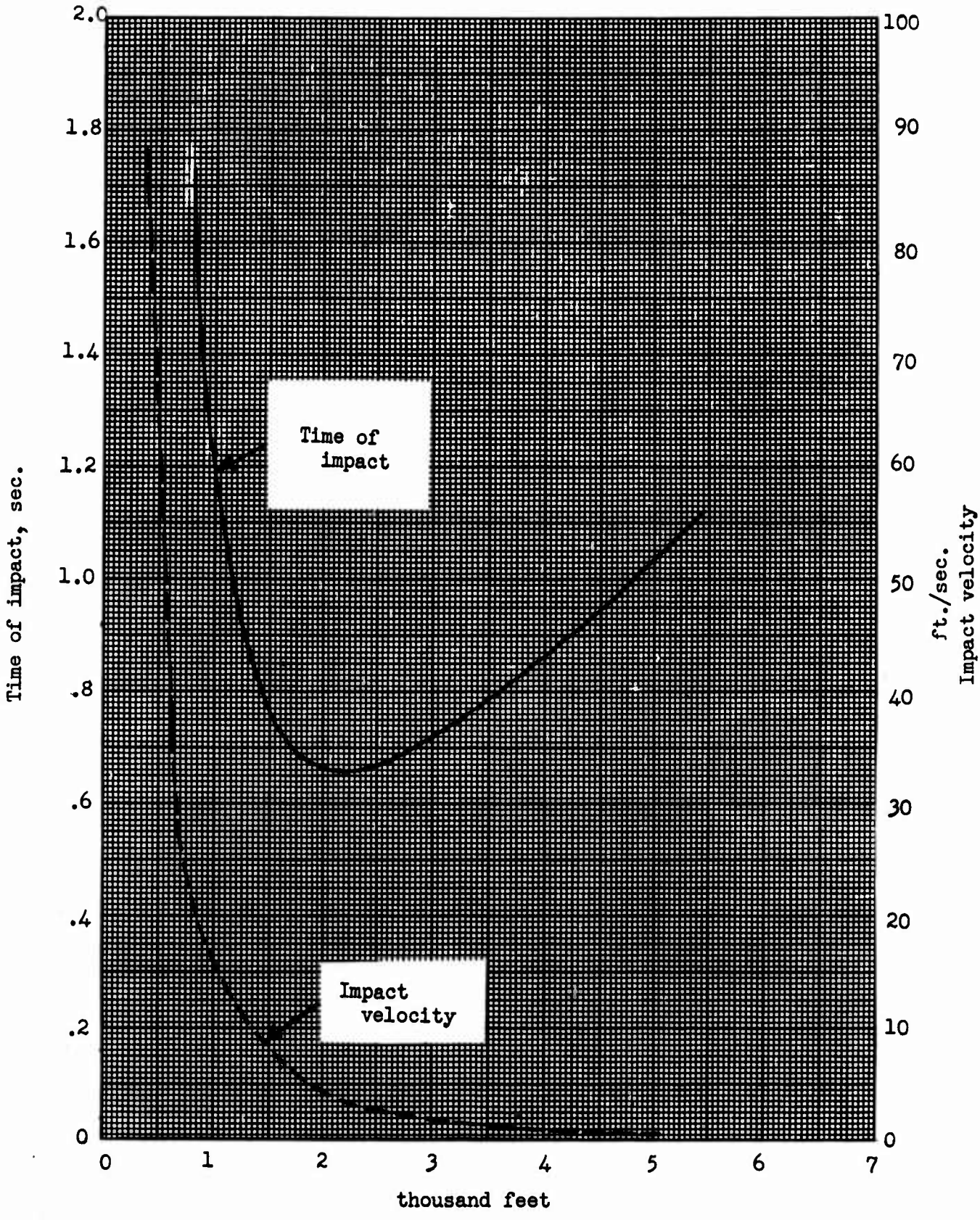

Fig. 24--Time of impact and impact velocity versus horizontal distance for a 10 KT yield at 200 foot depth.

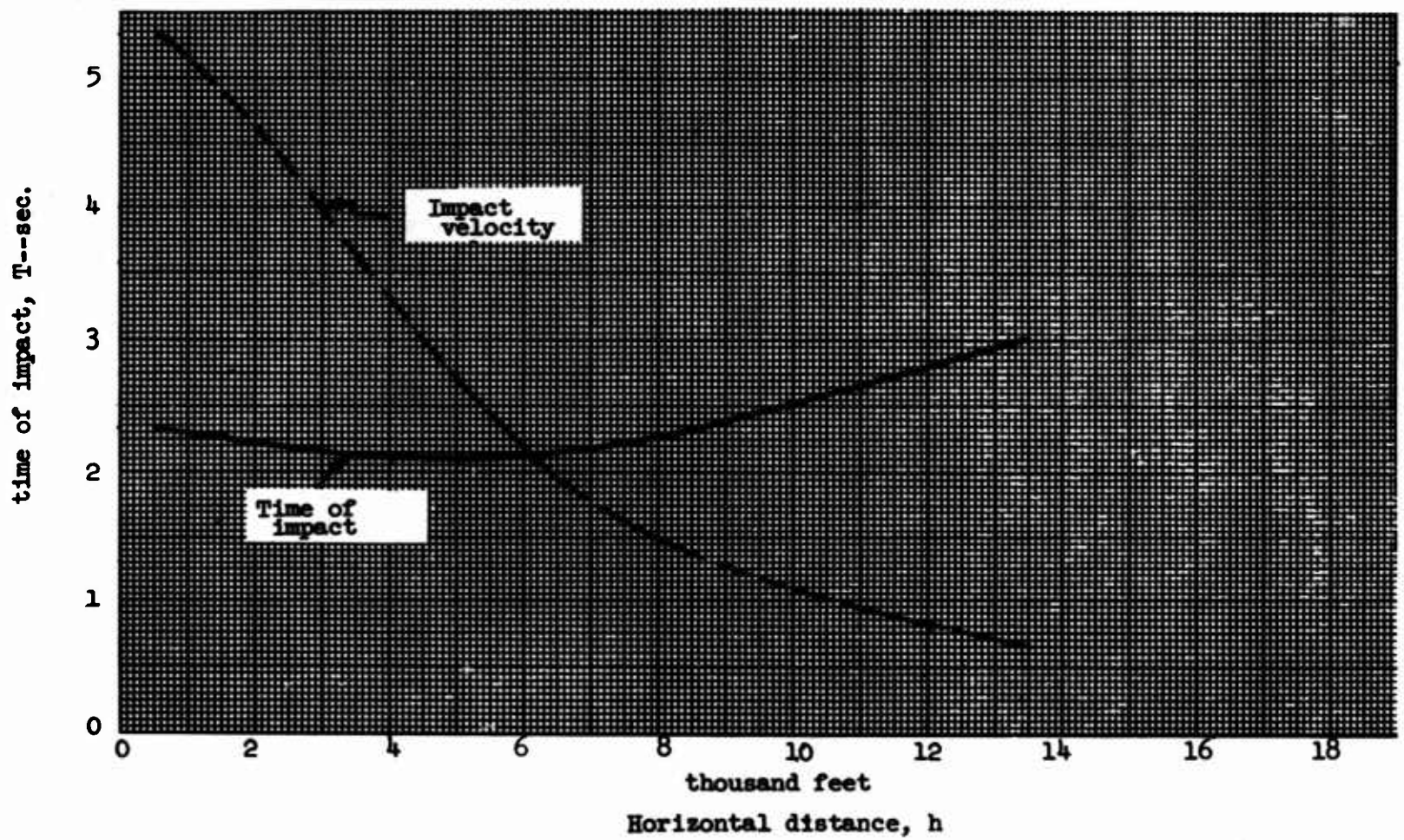

Fig. 25--Time of impact and impact velocity versus horizontal distance for a 20 K.T. yield at 5000-foot depth.

In all of the above cases except the 5000-foot depth shot the closing velocity from the circle of first impact is initially unbounded in both directions. The closing velocity then approaches the sound speed of water in the horizontal direction away from the bomb while the closing velocity in the direction toward the bomb soon decreases to rather low subsonic values and then again rises to an unbounded value as the water hammer approaches a point directly under surface zero. In the case of the 5000-foot depth shot the inward traveling water hammer did not go subsonic but rather reached a supersonic minimum. Other details of closure for the 5000-foot depth shot were similar to those of the other shots investigated.

In order to substantiate the use of this simplified model, calculations were made which could be compared with experimental data[5]. A satisfactory agreement between experimental and theoretical results was obtained.

---

[5]E. Swift, Jr., et al, "Underwater Pressures from Underwater Bursts," Operation HARDTACK, Proj. 1.1, WT-1606, U. S. Naval Ordnance Laboratory, August 15, 1960.

VI. SECONDARY WAVE CONFIGURATION

Section V has described the trajectory of the point of reloading. This traveling impact point is essentially a moving sound source or pressure source, and so we now investigate at least qualitatively the secondary wave patterns to be expected from such a moving source.

Figure 26a schematically indicates the secondary wave pattern soon after the time of first impact. Near the time of first impact, both the inward traveling as well as the outward traveling water hammers are moving supersonically (relative to sound speed in seawater). Indeed, analysis with Eq. (35) as indicated in Section V indicates that the outward traveling hammer is always traveling supersonically, but at an ever decreasing rate, asymptotically approaching sound speed. Consequently, typically, as indicated in Fig. 26a this supersonically traveling water hammer may be expected to produce a "bow shock." This bow shock or Mach line is at an angle β, as indicated in Fig. 26a, described by

$$\beta = \text{arc sin } 1/M \quad , \qquad (38)$$

where M is the Mach number of the traveling locus of impact. The inward traveling locus of impact also initially moves at a very high Mach number. The Mach lines due to these two traveling impact loci form a secondary shock wave as indicated in Fig. 26a. As long as both traveling impact points are moving supersonically, the associated secondary wave will have a shock front.

In Fig. 26b we indicate the secondary wave pattern at a somewhat later time, in fact at a time when the velocity of the inward traveling impact point has fallen well below sound speed. Most of the secondary wave configuration

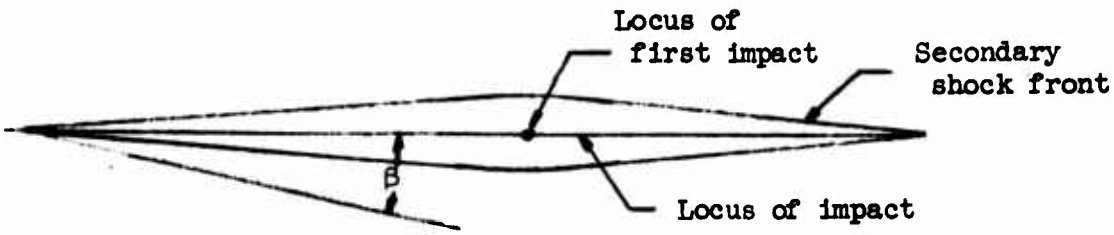

Fig. 26a--Secondary wave soon after the time of first impact.

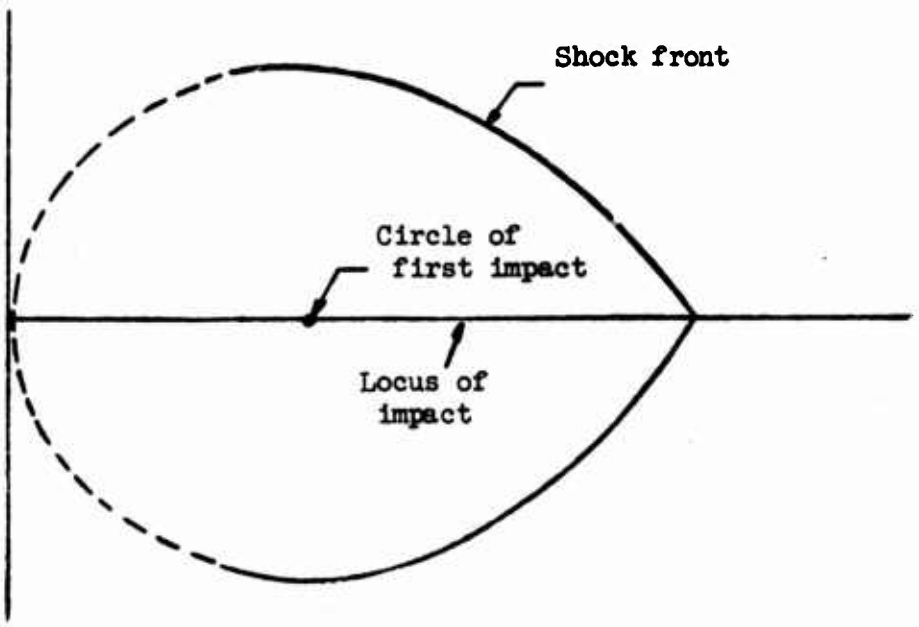

Fig. 26b--Secondary pressure wave at a time when the inward traveling impact point has fallen well below sound speed.

still has a shock rise, since these portions of the secondary wave were produced while both water hammers were still traveling supersonically. But that portion of the secondary wave which was generated while the inward traveling water hammer was moving at less than sound speed, will not have a shock rise appearance, but rather will have a gradual rise or precursor type of characteristic.

In Fig. 26b we indicate that the Mach lines due to the outward traveling hammer produce wave fronts which are pointed radially outward. On the other hand, the inward traveling water hammer--which, we have seen above, produces much more intense secondary waves--produces wave fronts which are traveling inward. That portion of the secondary wave configuration which is generated by the inward traveling water hammer tends to drive or focus secondary hydrodynamic wave energy toward two regions lying on the vertical axis passing through the explosion point: one point would appear to lie beneath the explosion point; while the other point would appear to be well above the explosion point. It is the latter region of concentration which is most meaningful in regard to the airblast above an underwater nuclear explosion.

In regard to the inward traveling water hammer it is interesting to call attention to the very strong Mach li[illegible] focusing effects which occur when a sound source or pressure source is accelerating or decelerating through the trans-sonic region. This is the "sonic boom" phenomenon which has been widely experienced and theoretically substantiated.[6]

---

[6] R. A. Struble, C. E. Stewart, E. A. Brown and A. Ritter, "Theoretical Investigations of Sonic Boom Phenomena," Armour Research Foundation of Illinois Institute of Technology for Wright Air Development Center, August 1957.

VII. SUMMARY

The previous one-dimensional analysis of bulk cavitation is being extended to the three-dimensional analysis. In the present report, results of a detailed analysis of the extent of the region of cavitation and a rudimentary analysis of the closure process are presented.

The detailed analysis shows that the cavitated region is much more extensive than it would appear to be in the traditionally accepted model. In particular, the cavitated region in our analysis may extend directly under the burst point. Although our analysis to date has neglected the gas globe at the burst point (and the physical existence of the gas globe will undoubtedly have a significant effect on cavitation directly beneath the burst point), it must be remembered that cavitation forms quickly and at an early time when the effect of gas globe is small. Thus, while the analytic result must be considered to be approximate directly under the burst point, it should be sufficiently accurate in nearby regions. The newly discovered shape of the cavitated region may have a significant effect on the water hammer since a large proportion of the water hammer energy is concentrated near the burst point. Therefore, it is believed that development of the more accurate estimate of the extent of the cavitating region, as presented here, will greatly improve the overall theory of water hammer.

In an effort to keep our initial models simple, we have not yet considered bottom effects. Consequently models may be considered accurate representations of explosions in deep water, (or of explosions on a rigid bottom), but the results must be modified to represent effects of explosions in shallow water. The necessary modifications will be developed in the continuing work.

The rudimentary analysis of closure presented in this report agrees satisfactorily with experimental results of large scale explosions and indicates that the major effects of the water hammer may be susceptible to approximation with a simplified theory for these cases. This preliminary analysis, however, does not consider the effect of atmospheric pressure on closure and it is expected that in small explosions, this effect will be important and thus require more refined analysis. It is interesting to note that this preliminary analysis assumes that the surface will have returned to its initial position at the time of closure. Since the theory seemingly agrees with experimental results (at least for larger explosions), it appears that distortions of the surface at the time of closure must be small.

The estimate of the secondary wave pattern based on this rudimentary closure analysis indicates that for most explosions initial impact will occur along a ring some (horizontal) distance from the burst point. Closure or water hammer will then proceed both radially inward and outward. The outward speed of closure will always be supersonic. However, except for very deep explosions, the inward speed of the traveling water hammer will initially be supersonic, then become subsonic and again rise to supersonic as surface zero is approached. As a result, the "sonic boom" phenomena will exist with an impulsive release of energy "focused" to the vertical line through the burst point.